

# Microbial symbionts buffer hosts from the demographic costs of environmental stochasticity

Joshua C. Fowler<sup>1,2\*</sup>, Shaun Ziegler<sup>3</sup>, Kenneth D. Whitney<sup>3</sup>,  
Jennifer A. Rudgers<sup>3</sup>, Tom E.X. Miller<sup>1</sup>

<sup>1</sup>\*Department of BioSciences, Rice University, Houston, 77005, TX, USA.

<sup>2</sup>Department of Biology, University of Miami, Miami, 33146, FL, USA.

<sup>3</sup>Department of Biology, University of New Mexico, Albuquerque, 87131, NM, USA.

\*Corresponding author(s). E-mail(s): [jcf221@miami.edu](mailto:jcf221@miami.edu);

Contributing authors: [shaun.ziegler@gmail.com](mailto:shaun.ziegler@gmail.com); [whitneyk@unm.edu](mailto:whitneyk@unm.edu);

[jrudgers@unm.edu](mailto:jrudgers@unm.edu); [tom.miller@rice.edu](mailto:tom.miller@rice.edu);

Phone: 719-359-2960

## Author Contributions

J.C.F. contributed to data collection, data analysis, and led manuscript drafting. S.Z. contributed to data collection and manuscript revisions. K.D.W. contributed to research conception, data collection, and manuscript revisions. J.A.R. established transplant plots, contributed to research conception, data collection, and manuscript revisions. T.E.X.M. contributed to research conception, data collection, data analysis, and manuscript revisions.

## Data and Code Accessibility

Data will be made accessible as an Environmental Data Initiative package online  
**DOI:** [updated here when available](#). Code for all analysis is available through  
<https://github.com/joshuacfowler/Grass-Endophyte-Stochastic-Demography>

**Article Type:** Letter

**Running Title:** Symbiont-mediated demographic buffering

**Keywords:** stochasticity, demography, symbiosis, mutualism, Epichloë, Testing the differences

**This file contains:** Abstract ( 150 words), Main Text (5397 words), Figures (1-4); Supporting Information - Supplemental Methods, Supplemental Figures A1-A28, Supplemental Tables S1-S3, References (66)

047      Manuscript submitted following PNAS style guidelines and can be  
048                  reformatted upon revision  
049  
050  
051  
052  
053  
054  
055  
056  
057  
058  
059  
060  
061  
062  
063  
064  
065  
066  
067  
068  
069  
070  
071  
072  
073  
074  
075  
076  
077  
078  
079  
080  
081  
082  
083  
084  
085  
086  
087  
088  
089  
090  
091  
092

**Abstract**

Species' persistence in increasingly variable climates will depend on resilience against the fitness costs of environmental stochasticity. Most organisms host microbiota that shield against stressors. Here, we test the hypothesis that, by limiting exposure to environmental extremes, microbial symbionts reduce hosts' demographic variance. We parameterized stochastic models using data from a 14-year symbiont-removal experiment including seven grass species that host *Epichloë* fungal endophytes. Endophytes reduced variance in fitness by > 10%, on average. Hosts with "fast" life history traits that lacked longevity as an intrinsic buffer benefited most from symbiont-mediated variance buffering. Under current climate conditions, contributions of variance buffering were modest compared to symbiont benefits to mean fitness. However, simulations of increased stochasticity amplified benefits of variance buffering and made it the more important pathway of host-symbiont mutualism than elevated mean fitness. Microbial-mediated variance buffering is likely an important, yet cryptic, mechanism of resilience in an increasingly variable world.

093	
094	
095	
096	
097	
098	
099	
100	
101	
102	
103	
104	
105	
106	
107	
108	
109	
110	
111	
112	
113	
114	
115	
116	
117	
118	
119	
120	
121	
122	
123	
124	
125	
126	
127	
128	
129	
130	
131	
132	
133	
134	
135	
136	
137	
138	

139 **Introduction**

140  
141 Global climate change involves increases in environmental variability, including  
142 changes to precipitation patterns and the frequency of extreme weather events [1, 2].  
143 Yet, the ecological consequences of increased variability are less well understood than  
144 those of changing climate means, such as long-term warming or drying. Incorpor-  
145 rating environmental variability into forecasts of population dynamics can improve  
146 predictions of the future.

147 Classic theory predicts that long-term population growth rates (equivalently, pop-  
148 ulation mean fitness) will decline under increased environmental stochasticity because  
149 the costs of bad years outweigh the benefits of good years – a consequence of nonlinear  
150 averaging [3, 4]. For example, in unstructured populations, the long-term stochastic  
151 growth rate in a fluctuating environment ( $\lambda_s$ ) will always be lower than the average  
152 growth rate ( $\bar{\lambda}$ ) by an amount proportional to the environmental variance ( $\sigma^2$ ):

153  
154 
$$\log(\lambda_s) \approx \log(\bar{\lambda}) - \frac{\sigma^2}{2\bar{\lambda}^2} \quad (1)$$
  
155

156  
157 Populations structured by size or stage similarly experience costs of variability [5, 6].  
158 There are accordingly two pathways to increase population viability in a variable  
159 environment: increase the mean growth rate and/or dampen temporal fluctuation in  
160 growth rates, also called “variance buffering”.

161 Both the characteristics of species and the properties of their environment can  
162 buffer demographic fluctuations, including life history traits such as longevity [7, 8],  
163 correlations among vital rates [9], transient shifts in population structure [10], the  
164 magnitude of environmental variability [11], or the degree of environmental autocor-  
165 relation [12, 13]. These factors determine the risks of extinction faced by populations  
166 [14] and underlie management strategies promoting ecosystem resilience [15]. Yet little  
167 is known about how biotic interactions influence demographic variability or contribute  
168 to variance buffering [16].

169 Most multicellular organisms host symbiotic microbes that affect growth and per-  
170 formance [17, 18], and many of these are vertically transmitted from maternal hosts to  
171 offspring [19]. Vertical transmission links the fitness of hosts and symbionts in a feed-  
172 back loop that selects for mutual benefits [20]. Many vertically-transmitted microbes  
173 are mutualistic and protect hosts from stressful environmental conditions including  
174 drought, extreme temperatures, or natural enemies [21, 22]. Some of the best studied  
175 examples include bacterial symbionts of insects that provide their hosts with thermal  
176 tolerance through the production of heat-shock proteins [23], and fungal symbionts of  
177 plants that produce anti-herbivore and drought-protective compounds [24–26]. How-  
178 ever, these diverse protective symbioses are context-dependent: the magnitude of  
179 benefits depends on environmental conditions [27] and thus will vary temporally in  
180 a stochastic environment [28]. We hypothesized that context-dependent benefits from  
181 symbionts may buffer hosts against variability through strong benefits during harsh  
182 periods and neutral or even costly outcomes during benign periods, reducing the  
183 impacts of host exposure to extremes and dampening inter-annual variance relative  
184 to non-symbiotic hosts. Variance buffering is a previously unexplored mechanism by

which symbionts may benefit their hosts instead of or in addition to elevating average fitness, the focus of most previous research.	185
	186
To test the hypothesis that context-dependent benefits of symbiosis buffer hosts from the fitness costs of environmental stochasticity, we used a combination of long-term field experiments and stochastic demographic modeling. We used cool-season grasses and <i>Epichloë</i> fungal endophytes as a tractable experimental model in which non-symbiotic plants can be derived from naturally symbiotic plants through heat treatment, providing a contrast of symbiont effects that controls for the confounding influence of host genetic background. <i>Epichloë</i> endophytes are specialized symbionts growing intercellularly in the aboveground tissue of ~ 30% of <i>C<sub>3</sub></i> grass species [29]. These fungi are primarily transmitted vertically from maternal plants through seeds [30]. They produce a variety of alkaloids that can protect host plants from natural enemies [31] and drought stress [32].	187
	188
	189
	190
	191
	192
	193
	194
	195
	196
	197
Over 14 years (2007–2021), we collected longitudinal demographic data on the survival, growth, reproduction, and recruitment of all plants within replicated endophyte-symbiotic and endophyte-free populations at our field site in southern Indiana, USA. Through taxonomic replication (seven host-symbiont species pairs) we aimed to understand whether host life history traits could explain inter-specific variation in the magnitude of demographic buffering through symbiosis. We used this long-term data to parameterize stochastic population projection models in a hierarchical Bayesian framework. Specifically, we (1) quantified the effect of symbiosis on the mean and variance of host vital rates (survival, growth and reproduction) and fitness, (2) evaluated the relationship between host life history traits and the magnitude of symbiont-mediated variance buffering, (3) determined the relative contribution of symbiont-mediated mean and variance effects to host fitness, and (4) projected how increased environmental stochasticity (expected under future climates) changes the importance of variance buffering as a pathway of host-symbiont mutualism.	198
	199
	200
	201
	202
	203
	204
	205
	206
	207
	208
	209
	210
	211
	212
<b>Materials and Methods</b>	213
<b>Study site and species</b>	214
This study was conducted at Indiana University's Lilly-Dickey Woods Research and Teaching Preserve (39.238533, -86.218150) in Brown County, Indiana, USA. This site is part of the Eastern broadleaf forests of southern Indiana, where the ranges of many understory cool-season grass species overlap. The experiment focused on seven of these grasses ( <i>Agrostis perennans</i> , <i>Elymus villosus</i> , <i>Elymus virginicus</i> , <i>Festuca subverticillata</i> , <i>Lolium arundinaceum</i> , <i>Poa alsodes</i> , and <i>Poa sylvestris</i> ), each of which hosts a unique species of <i>Epichloë</i> endophyte (Table S1). All are native to eastern North America except the Eurasian species <i>L. arundinaceum</i> .	215
	216
	217
	218
	219
	220
	221
	222
	223
	224
	225
<b>Endophyte removal, plant propagation, and field set-up</b>	226
Seeds from naturally symbiotic populations of the seven focal host species were collected during summer-fall 2006 from Lilly-Dickey Woods and the nearby Bayles Road Teaching and Research Preserve (39.220167, -86.542683). To generate symbiotic (S+)	227
	228
	229
	230

231 and symbiont-free (S-) plants from the same genetic lineages, seeds from each species  
232 were disinfected with a heat treatment described in Table S1 or left untreated. The heat  
233 treatment created symbiont-free plants by warming seeds to temperatures at which the  
234 fungus becomes inviable but the host seeds can still germinate. Both heat-treated and  
235 untreated seeds were surface sterilized with bleach to remove epiphyllous microbes,  
236 cold stratified for up to 4 weeks, then germinated in a growth chamber before transfer  
237 to the greenhouse at Indiana University where they grew for ~ 8 weeks. We confirmed  
238 endophyte status by staining thin sections of inner leaf sheath with aniline blue and  
239 examining tissue for fungal hyphae at 200X magnification [33]. We established exper-  
240 imental populations with vegetatively propagated clones of similar sizes. By starting  
241 the experiment with plants of similar sizes and the same number of unique genotypes,  
242 we aimed to limit any potential effects of heat treatments on initial plant growth [34].

243 During the fall of 2007 and spring of 2008, we established 10 3x3 m. plots for *A.*  
244 *perennans*, *E. villosus*, *E. virginicus*, *F. subverticillata*, and *L. arundinaceum* and 18  
245 plots for *P. alsodes* and *P. sylvestris*. Half of the plots were randomly assigned to be  
246 planted with either symbiotic (S+) or symbiont-free (S-) plants, and initiated with  
247 20 evenly spaced individuals labeled with aluminum tags. In spring 2008, we placed  
248 plastic deer net fencing around each plot to limit deer herbivory and disturbance;  
249 damaged fences were regularly replaced.  
250

## 251 **Long-term demographic data collection**

252 Each summer (2008–2021) we censused all individuals in each plot for survival,  
253 growth and reproduction, and added new recruits to the census. Plots contained 13.3  
254 individuals/m<sup>2</sup> on average over the course of the experiment. Each census year was a  
255 sample of inter-annual climatic variation (n = 14 years, comprising 13 demographic  
256 transition years). We censused each species during its peak fruiting stage (May: *Poa*  
257 *alsodes*, *Poa sylvestris*; June: *Festuca subverticillata*; July: *Elymus villosus*, *Elymus vir-*  
258 *ginicus*, *Lolium arundinaceum*; September: *Agrostis perennans*), such that the censuses  
259 were pre-breeding and new recruits came from the previous years' seed production.  
260 Leaf litter was cleared out of each plot prior to the census, to aid in locating plants.  
261 For each plant remaining from the previous year, we determined survival, measured  
262 its size as a count of tillers, and collected reproductive data as counts of reproductive  
263 tillers and seed-bearing spikelets on all reproductive tillers to a maximum of three. We  
264 also tagged all unmarked individuals that were recruits from the previous years' seed  
265 production and collected the same demographic data. New recruits typically had one  
266 tiller and were non-reproductive. In 2008 through 2010, we took additional counts of  
267 seeds per inflorescence for all reproducing individuals in the plots to relate inflorescence  
268 and spikelet counts to seed production. In 2018, we stopped collecting data for the  
269 exotic *L. arundinaceum*, which had very high survival and low recruitment, and conse-  
270 quently very low variation across years. In total across 14 years, the dataset included  
271 demographic information for 16,789 individual host-plants and 31,216 transition-year  
272 observations.  
273

274 We expected plots to maintain their endophyte status (symbiotic or symbiont-  
275 free) because these fungal symbionts are almost exclusively vertically transmitted,  
276 and plots were spaced a minimum of 5 m apart, limiting seed dispersal or horizontal

transmission of the symbiont between plots. However, we regularly confirmed endophyte treatment throughout the lifetime of the experiment by opportunistically taking subsets of seeds from reproductive individuals and scoring them for their endophyte status with microscopy as above. Overall, these scores reflected 98% faithfulness of recruits to their expected endophyte status across species and plots (Fig. S23; Supplement data). Additionally, we have rarely observed fungal stromata, the fruiting bodies by which *Epichloë* are potentially transmitted horizontally, provided the fly vector is also present [35]. For *A. perennans*, *F. subverticillata*, *L. arundinaceum*, and *P. alsodes*, we never observed stromata. We observed stromata only infrequently for *E. villosus*, and even more rarely for *E. virginicus* and *P. sylvestris* (Table S2). For these species, stromata have only been observed irregularly across years on 35, 4, and 6 plants respectively, making up < 0.3% of all censused plants.

## Vital rate modeling

Equipped with these demographic data, we fit statistical models for survival, growth, flowering (yes or no), fertility of flowering plants (number of flowering tillers), production of seed-bearing spikelets (number per inflorescence), the average number of seeds per spikelet, and the recruitment of seedlings from the preceding year's seed production. We fit these vital rates as generalized linear mixed models in a hierarchical Bayesian framework using RStan [36] which allowed us to isolate endophyte effects on vital rate means and variances, borrow strength across species for some variance components, and propagate uncertainty from the individual-level vital rates to population projection models [37]. All vital rate models included random plot and year effects, with separate estimates of year-to-year variance for symbiotic and symbiont-free plants, to quantify the effect of endophytes on inter-annual variance. All parameters were given vague priors [38]. We ran each vital rate model for 2500 warm-up and 2500 MCMC sampling iterations with three chains. We assessed model convergence with trace plots of posterior chains and checked for  $\hat{R}$  values less than 1.01, indicating low within- and between-chain variation [39, 40]. For those models that showed poor convergence, we extended the MCMC sampling to include 5000 warm-up and 5000 sampling iterations, which was only necessary for seedling growth. We graphically checked vital rate model fit with posterior predictive checks comparing simulated and observed data (Fig. S19-S20).

*Survival* - We modeled survival as a Bernoulli process, where the survival ( $S$ ) of an individual  $i$  in plot  $p$  and census year  $t$  was predicted by the plot-level endophyte status ( $e$ ), host species ( $h$ ), size in the preceding census, and the plant's origin status (whether it was initially transplanted or naturally recruited into the plot).

$$S_{i,p,e,h,t} \sim Bernoulli(\hat{S}_{i,p,e,h,t}) \quad (2a)$$

$$\text{logit}(\hat{S}_{i,p,e,h,t}) = \beta_{0_h} + \beta_1 * \text{origin}_i \quad (2b)$$

$$+ \beta_{2_h} * \text{endo}_e + \beta_{3_h} * \text{size}_{i,t-1} + \tau_{e,h,t} + \rho_p \quad (2c)$$

$$\tau_{e,h,t} \sim Normal(0, \sigma_{\tau_{e,h}}^2) \quad (2d)$$

323  $\rho_p \sim Normal(0, \sigma_\rho^2)$  (2e)  
 324

325 Here,  $\hat{S}$  is the survival probability,  $\beta_{0_h}$  is an intercept specific to each host species,  
 326  $\beta_1$  is the effect of the plant's recruitment origin,  $\beta_{2_h}$  is the endophyte effect,  $\beta_{3_h}$  is the  
 327 size effect,  $\tau_{e,h,t}$  is a normally distributed year effect for each species and endophyte  
 328 status with variance  $\sigma_{\tau_{e,h}}^2$ , and  $\rho_p$  is a normally distributed plot effect with variance  
 329  $\sigma_\rho^2$  ( $p(e)$  indicates that plot identity is uniquely associated with an endophyte status).  
 330 We assume that origin effect  $\beta_1$  and plot-to-plot variance  $\sigma_\rho^2$  are shared across host  
 331 species, allowing us to "borrow strength" across the multi-species dataset; other model  
 332 parameters are unique to host species. We separately modeled the survival of newly  
 333 recruited seedlings with a similar model but omitting previous size dependence and  
 334 origin status.

335 *Growth* - We modeled plant size in census year  $t$  ( $G$ ) with the same linear pre-  
 336 dictor for the mean as described for survival. Because we measured size as positive  
 337 integer-valued counts of tillers, we modeled it with a zero-truncated Poisson-inverse  
 338 Gaussian distribution. This distribution includes a shape parameter  $\lambda_G$  to account for  
 339 overdispersion in the data. We additionally modeled the growth of newly recruited  
 340 seedlings separately with a Poisson-inverse Gaussian model omitting size structure  
 341 and the plants' origin status as with seedling survival.

342 *Flowering* - We modeled whether or not a plant was flowering during the census ( $P$ )  
 343 as a Bernoulli process, with the same linear predictor for the mean as described above  
 344 for survival except that size dependence for reproductive vital rates was determined  
 345 by the individual's size during the same census year as opposed to its size during the  
 346 previous year.

347 *Fertility* - For a plant that was flowering during the census, its fertility was the  
 348 number of reproductive tillers produced ( $F$ ), which we modeled as a function of size in  
 349 the same census period with a zero-truncated Poisson-Inverse Gaussian distribution,  
 350 with the same linear predictor for the mean as described above.

351 *Spikelets per Inflorescence* - Spikelet production ( $K$ ) was recorded as integer counts  
 352 on up to three inflorescences per reproducing plant. We modeled these data with a neg-  
 353 ative binomial distribution, with the same linear predictor for the mean as described  
 354 above.

355 *Seed Production per Spikelet* - For individuals with recorded counts of seed pro-  
 356 duction, we calculated the number of seeds per spikelet from our counts of seeds and  
 357 spikelets per inflorescence, and then modeled seeds per spikelet ( $D$ ) as means of a  
 358 Gaussian distribution for each species and endophyte status. Because we had less  
 359 detailed data across years and plants for seed production than for other reproductive  
 360 vital rates, we omitted both plot and year random effects.

361 *Seedling Recruitment* - We used a binomial distribution to model the recruitment of  
 362 new seedlings ( $R$ ) into the plots from seeds produced in the preceding year, assuming  
 363 no long-lived seed bank. We included an intercept specific to each host and endophyte  
 364 status and the same random effects structure as in other models. We estimated the  
 365 number of seeds per plot in the preceding year by multiplying the total number of  
 366 reproductive tillers per plant by the mean number of spikelets per inflorescence and  
 367 mean number of seeds per spikelet ( $D$ ). For plants with missing fertility or spikelet

data, we used the expected number of reproductive tillers ( $F$ ) or of spikelets per inflorescence from ( $K$ ), drawing from the full posteriors of our models. We rounded this value to get the estimated seed production for each individual, and finally summed across all reproductive plants in each year and plot to get the total number of seeds produced.

## Stochastic population model

We parameterized stochastic matrix projection models using the fitted statistical vital rate models. Each matrix projection model included two state variables:  $r_t$  (the number of newly recruited individuals in year  $t$  which we assume to be non-reproductive), and  $\mathbf{n}_t$  (a vector including all non-seedling individuals of sizes  $x \in \{1, 2, \dots, U\}$ , ranging from one to the maximum number of tillers  $U$ ). We use these two state variables to avoid having to assume demographic equivalence between seedling and non-seedling one-tiller plants. We used the same model structure for each species and endophyte status (not shown in model notation for readability). See Fig. S21 for a generalized life cycle graph.

The number of recruits in year  $t + 1$  is given by:

$$r_{t+1} = \sum_{x=1}^U P(x; \boldsymbol{\tau}_P) F(x; \boldsymbol{\tau}_F) K(x; \boldsymbol{\tau}_K) D R(\boldsymbol{\tau}_R) n_t^x \quad (3)$$

The total number of seeds produced by a maternal plant of size  $x$  is the product of the size-specific probability of flowering  $P$ , the number of reproductive tillers  $F$ , the number of spikelets per inflorescence  $K$ , and the number of seeds per spikelet  $D$ . Multiplying by the probability of transitioning from seed to seedling  $R$  gives a per-capita rate of seedling production, which is multiplied by the number of plants of size  $x$  ( $n_t^x$ , the  $x^{\text{th}}$  element of  $\mathbf{n}_t$ ) and summed over all sizes. Each function also depends on the species- and endophyte-specific year random effects for that vital rate ( $\boldsymbol{\tau}$ , a vector of year-specific values derived from the statistical models).

The number of  $y$ -sized plants in year  $t + 1$  is given by:

$$n_{t+1}^y = Z(y; \boldsymbol{\tau}_Z) B(\boldsymbol{\tau}_B) r_t + \sum_{x=1}^U S(x; \boldsymbol{\tau}_S) G(x, y; \boldsymbol{\tau}_G) n_t^x \quad (4)$$

where  $n_{t+1}^y$  is the  $y^{\text{th}}$  element of vector  $\mathbf{n}_{t+1}$ . The first term on the right hand side of Eqn. 4 represents growth ( $Z$ ) and survival ( $B$ ) of seedling recruits. The second term includes the survival of previously  $x$ -sized plants and the growth of survivors from size  $x$  to  $y$ , summed over all  $x$ . To avoid predictions of unrealistic growth outside of the observed size distribution, we set a ceiling on the growth function for plants at the 97.5<sup>th</sup> percentile of observed sizes for each host species [41].

Each of the vital rate functions in Eqns. 3 and 4 have separate intercepts and year random effects for symbiotic and symbiont-free populations, allowing us to calculate the effect of endophyte symbiosis on the mean, variance, and coefficient of variation (CV) of  $\lambda$ , the dominant eigenvalue of the year- and endophyte-specific projection matrix. This model treats climate drivers implicitly through year-specific random

415 effects. We also developed a climate-explicit version with the addition of parameters  
 416 defining the relationship between either annual or growing season drought index and  
 417 each vital rate. A full description of climate-explicit methods can be found in the  
 418 *Supporting Information Supplemental Methods*.

419

## 420 Life History Analysis

421

422 We collected metrics describing each host species' life history to test the relationship  
 423 between pace of life and variance buffering (Table S1). Using the Rage package [42],  
 424 we calculated  $R_0$ , longevity, and generation time from the mean transition matrix for  
 425 symbiont-free populations. We recorded seed size as the average lemma length from  
 426 the Flora of North America [43]. We also calculated the 99th percentile of maximum  
 427 observed age for each species from their S- populations. Next, we fit Bayesian phy-  
 428 logenetic mixed-effects models using the brms package [44] to test the relationship  
 429 between each life history trait and the effect of symbiosis on the CV of  $\lambda$  (a measure of  
 430 variance buffering) while controlling for phylogenetic non-independence between host  
 431 and symbiont species. We pruned species-level phylogenies of plants [45] and *Epichloë*  
 432 fungi [46] to include the focal species. *Agrostis perennans* was not included in the tree,  
 433 and so we used the congener *A. hyemalis*. We defined separate phylogenetic covariance  
 434 matrices for each pruned tree. We propagated uncertainty in the estimated variance  
 435 buffering effect  $V$  with a measurement error model:

436

437

$$V_{MEAN,h} \sim Normal(V_{EST,h}, V_{SD,h}) \quad (5a)$$

438

$$V_{EST,h} \sim Normal(\mu_h, \sigma) \quad (5b)$$

439

$$\mu = \alpha + \beta * trait + \pi_j \quad (5c)$$

440

$$\alpha \sim Normal(0, .5) \quad (5d)$$

441

$$\beta \sim Normal(0, .1) \quad (5e)$$

442

$$\sigma \sim Half-Normal(.04, .01) \quad (5f)$$

443

$$\pi_h \sim MVN(0, \sigma_\pi \mathbf{A}) \quad (5g)$$

444

$$\sigma_\pi \sim Half-Normal(0, .1) \quad (5h)$$

445

446

447

448 Here,  $V_{EST}$  is the variance buffering effect for host species  $h$ , estimated from the  
 449 posterior mean ( $V_{MEAN}$ ) and standard deviation ( $V_{SD}$ ), propagating uncertainty asso-  
 450 ciated with the effect of symbiosis. The model includes an intercept ( $\alpha$ ) and a slope  
 451 ( $\beta$ ) defining the relationship between the variance buffering effect and the life history  
 452 trait. The residual standard deviation is given by ( $\sigma$ ). We used weakly informative  
 453 priors to aid model convergence. Each prior was centered at zero, except for the resid-  
 454 ual standard deviation, which we centered at the standard deviation of the estimated  
 455 variance buffering effect, .04. The phylogenetic random effect ( $\pi$ ), which is modeled  
 456 as a multivariate normal distribution, has a between-species standard deviation ( $\sigma_\pi$ )  
 457 structured by the phylogenetic covariance matrix  $\mathbf{A}$ . We ran each MCMC sampling  
 458 chain for 8000 warmup iterations and 2000 sampling iterations. We assessed model  
 459 convergence as described for the vital rate models.

460

<b>Mean-variance decomposition</b>	461
To calculate stochastic population growth rates ( $\lambda_s$ ) for each host species and endophyte status we simulated population dynamics for 1000 years by randomly sampling from the 13 annual transition matrices, discarding the first 100 years to minimize the influence of initial conditions. Sampling observed transition matrices produces models that realistically capture inter-annual variation by preserving correlations between vital rates [47]. We tallied the total population size at each time step as $N_t = r_t + \sum_{x=1}^U n_t^x$ and calculated the stochastic growth rate as $\log(\lambda_s) = E[\log(\frac{N_t}{N_{t+1}})]$ [48, 49]. We calculated the total effect of endophyte symbiosis as the difference in $\lambda_s$ between S+ and S- populations. We propagated uncertainty from the vital rate models to the calculation of $\lambda_s$ using 500 draws from the posterior distribution of model parameters.	462 463 464 465 466 467 468 469 470 471 472 473 474 475 476 477 478 479 480 481 482 483 484 485 486 487 488 489 490 491 492 493 494 495 496 497 498 499 500 501 502 503 504 505 506
We decomposed the total endophyte effect on $\lambda_s$ into contributions from effects on vital rate means, variances, and their interaction. Specifically, we repeated the calculation of $\lambda_s$ for two additional “treatments”: (1) endophyte effects on mean vital rates only, with inter-annual variances shared between S+ and S- at the S- reference level for all vital rates, and (2) endophyte effects on vital rate variances only, with vital rate means shared between S+ and S- at the S- reference level. The combination of all four $\lambda_s$ treatments (S+ vital rate means and variances, S- means and variances, S+ means with S- variances, S- means with S+ variances) allowed us to quantify to what extent the overall effect of symbiosis derives from changes in vital rates means, variances, and their interaction. The interaction occurs because the variance penalty to stochastic growth is proportional to the mean value of annual growth rates (see Eq. 1) such that variance is more detrimental for populations with lower average growth rates.	474 475 476 477 478 479 480 481 482 483 484 485 486 487 488 489 490 491 492 493 494 495 496 497 498 499 500 501 502 503 504 505 506
To create scenarios of increased variance relative to that observed during the study period, we repeated the stochastic growth rate decomposition, but sampling only subsets of the 13 observed annual transition matrices. We created two scenarios of increased environmental variance by sampling the transition matrices associated with the set of either six or two most extreme $\lambda$ values. These extreme $\lambda$ values represent the best and worst years experienced by the plants, using the S- populations as the reference condition. By sampling away from an average year in both directions, the six- and two- years scenarios increased the standard deviation of yearly host growth rates by 1.3 and 2.1 times, respectively, without changing mean growth rates (< 2.3% difference in $\bar{\lambda}$ between simulation treatments, Fig. S22). We performed the same mean-variance decomposition for these scenarios as for the ambient conditions (all 13 years sampled) for all host species described above.	474 475 476 477 478 479 480 481 482 483 484 485 486 487 488 489 490 491 492 493 494 495 496 497 498 499 500 501 502 503 504 505 506
<b>Results</b>	500
<b>Symbionts buffer host demographic variance</b>	501
Across seven host species, eight vital rates, 14 years, and 16,789 individual plants, our analysis provided the first empirical evidence of symbiont-mediated variance buffering. Endophytes reduced inter-annual variance for 66% (37/56) of host species-vital	502 503 504 505 506

507 rate combinations (average Cohen's D for effects on vital rate standard deviation:  
508 -0.15) (Fig 1A; Fig. S6 - Fig. S18). Endophytes also increased mean vital rates for  
509 the majority (36/56) of host species-vital rate combinations (average Cohen's D for  
510 effects on vital rate mean: 0.15), and benefits were particularly strong for host sur-  
511 vival, plant growth and recruitment (Fig. 1A; Fig. S1 - Fig. S5). The magnitude of  
512 mean and variance effects differed among host species and vital rates. For example,  
513 endophytes modestly increased mean adult survival (Fig. 1C) and reduced variance in  
514 survival (Fig. 1D) for *Festuca subverticillata*, while for *Poa alsodes*, variance buffer-  
515 ing was more apparent in seedling growth and inflorescence production (Fig 1E).  
516 Interestingly, certain vital rates showed costs of endophyte symbiosis. Symbiotic indi-  
517 viduals of *A. perennans* grew larger than those without endophytes (Fig. 1B), yet  
518 endophytes also reduced this species' mean recruitment rates (Fig. 1A). In addition,  
519 endophyte symbiosis increased variance in seedling growth for *Elymus villosus* and  
520 *Festuca subverticillata* (Fig. 1A).

521 Because not all vital rates contribute equally to fitness, we used stochastic matrix  
522 models to integrate the diverse effects on vital rates described above into comprehen-  
523 sive measures for the mean and variance of year-to-year fitness ( $\lambda_t$ ) and the long-run  
524 stochastic fitness that integrates both mean and variance ( $\lambda_S$ ). On average across host  
525 species, S+ populations had greater mean fitness (> 92% confidence that endophytes  
526 increased  $\bar{\lambda}$ ) and lower inter-annual variability in fitness (> 86% confidence that endo-  
527 phytes decreased the coefficient of variation of  $\lambda_t$ ) than S- populations (Fig. 2). For  
528 some host species, the CV of  $\lambda_t$  declined by as much as 170% (*P. alsodes*, *F. subverti-*  
529 *cillata*), while for others, endophyte effects on variance were substantially smaller (6%  
530 lower for *E. villosus*, 16% lower for *A. perennans*), or even positive (27% increase for  
531 *E. virginicus*). When mean and variance effects of symbionts were considered together,  
532 none of the host-symbiont pairings were antagonistic (i.e., with endophytes that both  
533 decreased mean fitness and increased variance) (Fig. 2C), suggesting that variation  
534 across host species and vital rates in mean and variance effects may reflect alternative  
535 strategies that yield similar net benefits of endophyte symbiosis.

536 Reduced sensitivity to drought, as has been reported for some *Epichloë* symbioses  
537 [32], is a candidate mechanism that could generate a signature of variance buffering;  
538 drought conditions may have weaker fitness costs for S+ hosts, reducing fluctuations in  
539 fitness through time. Accordingly, analysis of climate-explicit matrix models indicated  
540 that, for five of seven taxa, S+ populations were less sensitive to annual or growing  
541 season drought (12-month or 3- month drought index; Standardized Precipitation-  
542 Evapotranspiration Index [50]) than S- populations (Supporting Information Text;  
543 Fig. S24-S25; Table S3). However, we did not find a strong relationship between the  
544 magnitude of variance buffering and relative drought sensitivities, suggesting that  
545 other climatic factors or other temporally-varying aspects of the environment may  
546 elicit benefits of endophyte symbiosis, including documented resistance to herbivory  
547 for six of these host taxa [51, 52].<sup>1</sup>

548

---

549 <sup>1</sup> This could potentially go in the discussion

550

551

552

## Faster life histories predict stronger symbiont-mediated variance buffering

Theory predicts that long-lived species, those on the slow end of the slow-fast life history continuum, will be less sensitive to environmental variability than short-lived species [53], a pattern which has empirical support across plants [54] and animals [8, 55]. Therefore, host species with long lifespans that produce few, large offspring should benefit less from symbiont-mediated variance buffering than species with fast life cycles that produce many smaller offspring with low per-capita chance of success [56, 57]. In support of this prediction, hosts with trait values representing faster life history strategies experienced greater variance buffering from endophytes than those with slow life histories (Fig. 3). Bayesian phylogenetic mixed-effects models, controlling for species' relatedness, indicated that variance buffering was stronger for host species with shorter lifespan (Fig. 3A; 75% probability of positive relationship with empirically observed maximum plant age) and smaller seeds (Fig. 3B; 73% probability of positive relationship with seed length). Other life history traits similarly had positive, but weaker, support for the prediction that faster life history traits correlate with stronger variance buffering (Fig. S26-S28). Considering fungal life history traits, the three host species for which the net mutualism benefit was weakest (*Elymus villosus*, *Elymus virginicus*, and *Poa sylvestris*) (Fig. 2C) were the only hosts for which we observed fungal stromata, fruiting bodies capable of horizontal (contagious) transmission (Table S2). This result supports the theoretical expectation that strict vertical transmission drives the evolution of strong host-symbiont mutualism [20, 58]. Conclusions about life histories are somewhat constrained by the narrow range of trait values among closely related species in the grass sub-family Pooideae and their co-evolving symbionts. Our understanding of how life history variation modulates the fitness consequences of microbial symbiosis would profit from tests across a wider span of taxonomic groups [59].

## Contributions from variance buffering are weak relative to mean effects

To evaluate the relative importance of mean fitness benefits and variance buffering as alternative pathways of mutualism, we decomposed the overall effect of the symbiosis on the stochastic growth rate  $\lambda_S$  using simulations from the population models in four configurations. These included either the full symbiosis effect (both mean and variance buffering effects), mean effects alone, variance effects alone, or neither mean nor variance effects. Overall, the full effect of symbiosis on  $\lambda_S$ , averaged across host species, provided strong evidence of grass-endophyte mutualism (99% certainty of a positive total effect on  $\lambda_s$ ) (Fig. 4; see Fig. S22 for individual host species). Contributions to this full effect derived from both mean and variance buffering effects, as well as a slightly negative interaction (i.e., the combined influence of mean and variance effects was smaller than the sum of their individual effects). Endophytes' contributions to  $\lambda_S$  from mean effects were four times greater, averaged across species, than contributions from variance buffering (Fig. 4), suggesting that, under the regime of environmental variability represented by our 14-year study, damped fluctuations in fitness via

599 variance buffering was a far less important element of the benefits of symbiosis than  
600 increased mean fitness. Results for individual host species were largely consistent with  
601 the cross-species trends (Fig S22). The full effect of symbiosis on  $\lambda_S$  was positive for  
602 seven out of eight host species, with statistical confidence ranging from 66% to > 99%  
603 certainty. The one exception was the host species *P. sylvestris*, for which our analysis  
604 indicated that fungal endophytes were effectively neutral in their overall fitness effect  
605 (45% and 55% posterior probability of positive and negative effects; Fig S22).

606

## 607 **Variance buffering strengthens under increased environmental 608 variability**

609

610 Simulations of increased environmental variability, a key prediction of climate change  
611 forecasts [2], indicated that mutualism with microbial symbionts, and their variance  
612 buffering effects in particular, will take on increased importance for hosts in a more  
613 variable future climate. To simulate increased variability, we repeated the decomposi-  
614 tion of  $\lambda_S$  for two alternative forecast scenarios, randomly sampling transition matrices  
615 that represented either the six most extreme years experienced by each species or the  
616 two most extreme years, subsets of the thirteen transition matrices across the 14-year  
617 study period. Increased variability elicited stronger mutualistic benefits of endophyte  
618 symbiosis (Fig. 3) than ambient variability (overall effect of the symbiosis increased  
619 by > 130%). This increase was driven by increased contributions from the variance  
620 buffering mechanism (from a 24% contribution in the ambient scenario to a 66% con-  
621 tribution in the most variable scenario) rather than from greater mean effects. In the  
622 most variable scenario, the relative importance of mean and variance effects reversed,  
623 with variance buffering contributions that were 1.5 times greater than contributions  
624 from mean benefits, averaged across species (Fig. 4). Thus, variance buffering – a cryp-  
625 tic microbial influence that manifests only over long time scales – is poised to become  
626 the dominant way in which grasses benefit from symbiosis with fungal endophytes in  
627 more variable climates of the future.

628

## 629 **Discussion**

630

631 - The fact that this is a field experiment in one location - Evolutionary context: i.e.  
632 different alternative strategies of mean and variance; diverse microbiome, bet-hedging

633

## 634 **Conclusion**

635

636 Ecologists increasingly recognize the importance of symbiotic microbes for host organ-  
637 isms and the populations, communities, and ecosystems in which their hosts reside  
638 [60–63]. Despite awareness of these ubiquitous interactions, long-term studies of micro-  
639 bial symbiosis are very rare. Our analysis of taxonomically-replicated, long-term field  
640 experiments that manipulated the presence/absence of fungal symbionts in plants  
641 demonstrates for the first time that heritable microbes can commonly benefit hosts  
642 not only through improved mean fitness – the focus of most previous research – but  
643 also through buffering against environmental variance. Our results provide an impor-  
644 tant advance to improve forecasts of the responses of populations (and symbionts)

to increasing environmental stochasticity under global change, suggesting that, for  
some host species, microbial symbiosis may compensate for the lack of intrinsic toler-  
ance of variability conferred by “slow” life history traits. We found that, relative to  
mean fitness benefits, symbiont-mediated variance buffering made weak contributions  
to host-symbiont mutualism under the current regime of environmental variability.  
However, variance buffering is likely to become the dominant benefit that fungal  
endophytes confer to grass hosts in more variable future environments. This result  
emerges from the context-dependent nature of grass-endophyte interactions, combined  
with the observation that environmental stochasticity generates fluctuation in con-  
text. These key ingredients, and thus the potential for symbiont-mediated variance  
buffering, similarly apply to the diverse host-microbe symbioses across the tree of life.

645  
646  
647  
648  
649  
650  
651  
652  
653  
654  
655  
656  
657  
658  
659  
660  
661  
662  
663  
664  
665  
666  
667  
668  
669  
670  
671  
672  
673  
674  
675  
676  
677  
678  
679  
680  
681  
682  
683  
684  
685  
686  
687  
688  
689  
690

691 **Acknowledgments.** We thank Mark Sheehan, Ali Campbell, Kyle Dickens, Blaise  
692 Willis, and Sar Lindner for contributions to field data collection. We also thank Volker  
693 Rudolf, Daniel Kowal, Lydia Beaudrot and Judie Bronstein for helpful comments on  
694 and discussion of this project. This research was supported by the National Science  
695 Foundation (grants 1754468 and 2208857).

696 **Supplementary information.** Supplementary information for this paper includes  
697 Supplementary Methods, Figs. A1 to A28, and Tables A1 to A3.  
698

699

700

701

702

703

704

705

706

707

708

709

710

711

712

713

714

715

716

717

718

719

720

721

722

723

724

725

726

727

728

729

730

731

732

733

734

735

736

## Figures

737

738

739

740

741

742

743

744

745

746

747

748

749

750

751

752

753

754

755

756

757

758

759

760

761

762

763

764

765

766

767

768

769

770

771

772

773

774

775

776

777

778

779

780

781

782

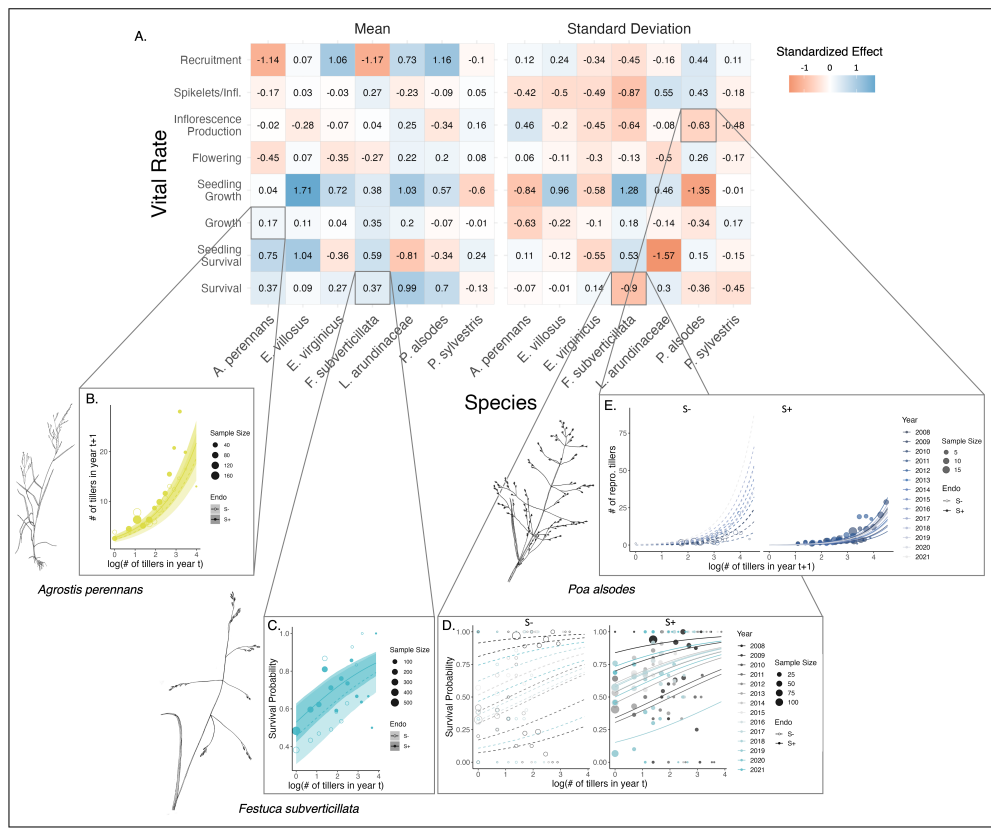
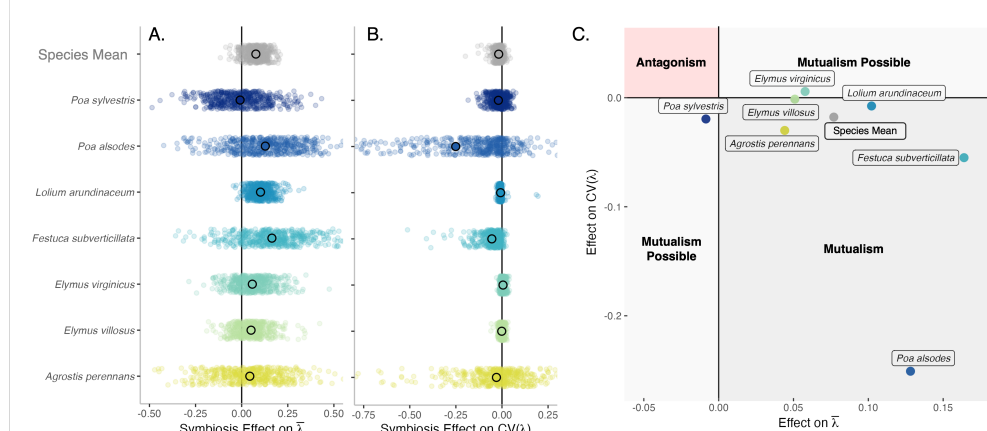


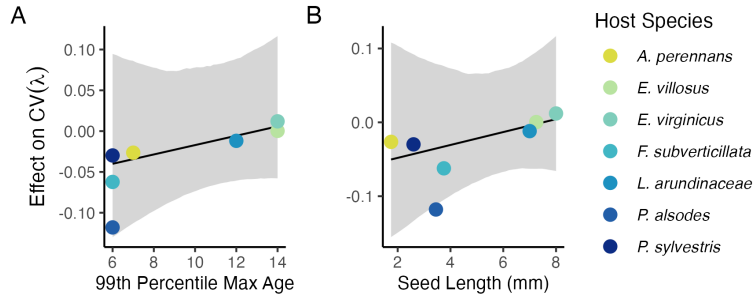
**Fig. 1** Endophyte symbiosis altered host vital rates.(A) Shading represents the posterior mean standardized effect size (Cohen's D) of endophyte symbiosis on mean or standard deviation of host vital rates (blue indicates that symbiosis increased the mean or standard deviation and red indicates a reduction). Endophytes' diverse vital rate effects include increased (B) mean growth of *A. perennans* and (C) mean survival probability of *F. subverticillata*. Endophyte presence also reduced inter-annual variance in (D) the survival of *F. subverticillata* and (E) the fertility of *P. alsodes*. In panels B-C, mean vital rate estimates are shown with 80% credibles along with data binned by size for symbiotic (S+) and symbiont-free (S-) plants, while in panels D-E, annual vital rate estimates are shown along with data binned by size and census year. Organism silhouettes modified from "Festuca subverticillata" by Cindy Roché and "Agrostis hyemalis" and "Poa alsodes" by Sandy Long ©Utah State University.

783  
784  
785  
786  
787  
788  
789  
790  
791  
792  
793  
794  
795  
796  
797  
798  
799



800  
801 **Fig. 2** Mean and variance-buffering effects on fitness. Black circles indicate the average effect of  
802 endophytes along with 500 posterior draws (smaller colored circles) on the (A) mean and (B) coeffi-  
803 cient of variation in  $\lambda$  for each host species as well as a cross species mean. (C) For all hosts,  
804 endophytes either reduce variance, increase the mean, or both, and consequently when considering  
805 stochastic environments, the interactions are always at least potentially mutualistic.

806  
807  
808  
809  
810  
811  
812  
813  
814  
815  
816  
817  
818  
819  
820  
821



822 **Fig. 3** Host species with faster life history traits experience stronger effects of symbiont-mediated  
823 variance buffering. Regressions between life history traits describing the fast-slow life history contin-  
824 uum ((A) 99th percentile maximum age observed during long term censuses in years; (B) Seed size)  
825 and the effect of endophyte symbiosis on the coefficient of variation in population growth rate ( $\lambda$ ).  
826 Each panel shows the fitted mean relationship (line) along with the 95% credible interval.  
827  
828

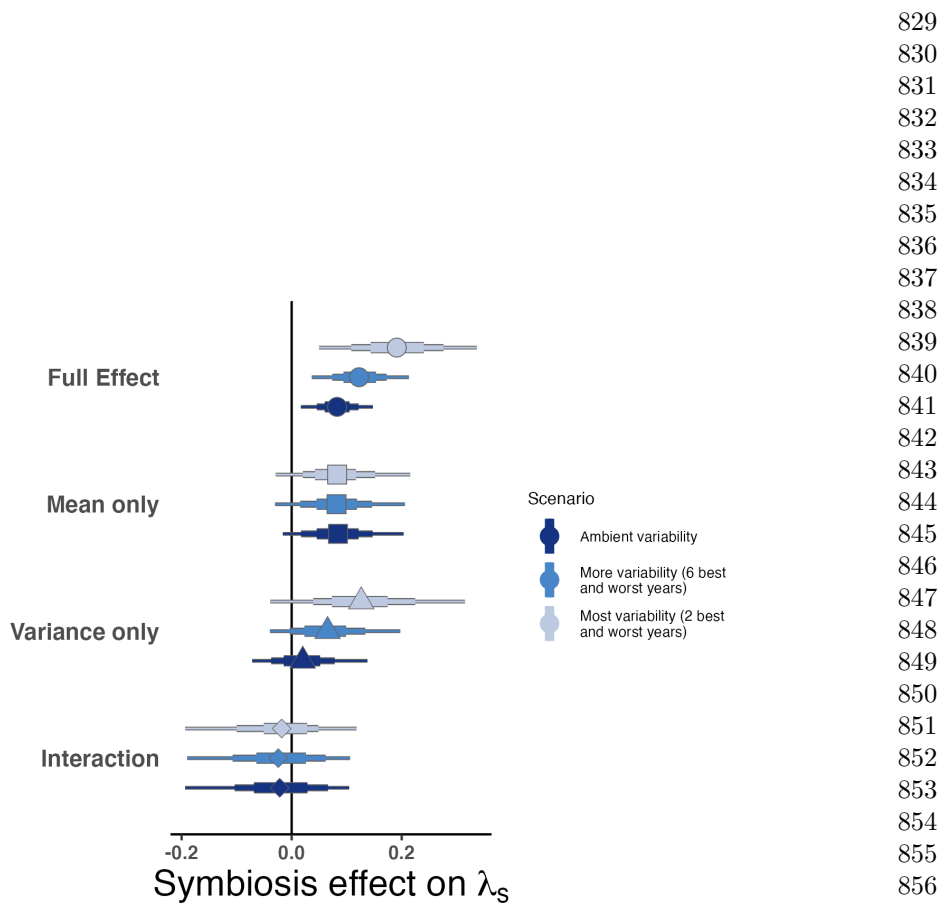


**Fig. 4** Cross-species average endophyte contributions to stochastic growth rates under observed and elevated variance. Endophyte symbiosis contributes to the total effect of mutualism on  $\lambda_S$  through benefits to mean growth rates and through variance buffering as well as the interaction between mean and variance effects. Shapes indicate the posterior mean of each contribution averaged across the seven focal symbiota, along with bars for the 50, 75 and 95% credible intervals. The full effect of the symbiosis (circles) becomes more mutualistic under scenarios of increased variance (represented by color shading). Relative to the ambient scenario sampling transition matrices for all 13 transition years during the study period, simulations increased variance by sampling the most extreme six or two years years, leading to increased contributions from variance buffering effects (triangles) and a constant contribution from mean effects (squares).

875 **Supporting Information**

876

877 **Supplemental Methods**

878 **Estimating climate drivers of environmental context-dependence**

879 To connect the variance buffering effects of endophytes with inter-annual variability  
880 in climate, we built climate-explicit stochastic matrix population models from the  
881 vital rate data in addition to the climate-implicit model described in the main text.  
882 Identifying the potentially complex relationships between vital rates and environmen-  
883 tal drivers remains a key challenge for accurate forecasts of the ecological impacts of  
884 environmental stochasticity [64]. We first downloaded temperature and precipitation  
885 data from a weather station in Bloomington, IN, approx. 27 km from our study site,  
886 using the rnoaa package [65]. Compared to other weather stations in the area, the  
887 measurements from Bloomington contain the most complete climate record across the  
888 study period and are correlated with more local measurements from Nashville, IN for  
889 years in which local data are available (total daily precipitation:  $R^2 = .76$ ; mean daily  
890 temperature:  $R^2 = .94$ ). The mean annual temperature across the study period was  
891  $11.9 C^\circ$  (SD:  $1.05 C^\circ$ ) and the average annual precipitation was  $1237.9 \text{ mm/year}$  (SD:  
892  $204.89 \text{ mm/year}$ ) (Fig. S24). Given the known role of endophytes in promoting host  
893 drought tolerance, we calculated the Standardised Precipitation-Evapotranspiration  
894 Index (SPEI) for 3 and 12 months preceding each annual censuses, reflecting drought  
895 during the growing season and across the year [50]. To calculate SPEI, we used the  
896 Thornthwaite equation to model potential evapotranspiration as implemented in the  
897 SPEI R package [66]

898 We repeated the process of fitting statistical models for each vital rate as described  
899 in **Materials and Methods** with the inclusion of a parameter describing the influ-  
900 ence of SPEI. We fit separate vital rate models incorporating either the growing season  
901 or annual drought index for each vital rate, except for the model describing the mean  
902 number of seeds per inflorescence. This model was fit without climate effects because  
903 the data came from only a few years. Initial analyses indicated similar fits for models  
904 including only a linear term and those with both linear and quadratic terms describ-  
905 ing the relationship between the climate driver and the vital rate response, and so  
906 we proceeded with models including only the linear term. We expected that includ-  
907 ing climate predictors into the models would explain some inter-annual variance in  
908 vital rates, shrinking the variance associated with the fitted year random effects. We  
909 assessed model fit with graphic posterior predictive checks and convergence diagnostics  
910 as described for the climate-implicit analysis. Finally, we next built matrix projec-  
911 tion models incorporating the climate-dependent vital rate functions to assess the  
912 response of symbiotic (S+) vs symbiont-free (S-) populations to drought. The model  
913 is as described in **Materials and Methods** with the inclusion of parameters describ-  
914 ing the slope of the relationship with SPEI. We compared the sensitivity of  $\lambda$  to either  
915 annual or seasonal SPEI of S+ populations ( $\frac{\Delta\lambda^+}{\Delta SPEI}$ ) with those of S- populations  
916 ( $\frac{\Delta\lambda^-}{\Delta SPEI}$ )(Fig. S25; Table S).

917 Most species were slightly more responsive to growing season rather than annual  
918 drought conditions, and for most species symbiotic populations were less sensitive to  
920

SPEI than symbiont-free populations (Fig. S25; Table S3). However, these drought	921
indices did not explain the full extent of inter-annual variability in demographic	922
vital rates. For example, flowering in <i>A. perennans</i> had one of the strongest climate	923
signals (82% probability of a positive relationship with SPEI), yet the estimated inter-	924
annual variance $\sigma_{\tau_P}^2$ for symbiont-free plants shrank from 6.7 to 6.1 after including	925
3-month SPEI as a covariate, suggesting that other factors contribute to inter-annual	926
variability.	927
	928
	929
	930
	931
	932
	933
	934
	935
	936
	937
	938
	939
	940
	941
	942
	943
	944
	945
	946
	947
	948
	949
	950
	951
	952
	953
	954
	955
	956
	957
	958
	959
	960
	961
	962
	963
	964
	965
	966

## 967 Supplemental Figures S1-S28

968

969

970

971

972

973

974

975

976

977

978

979

980

981

982

983

984

985

986

987

988

989

990

991

992

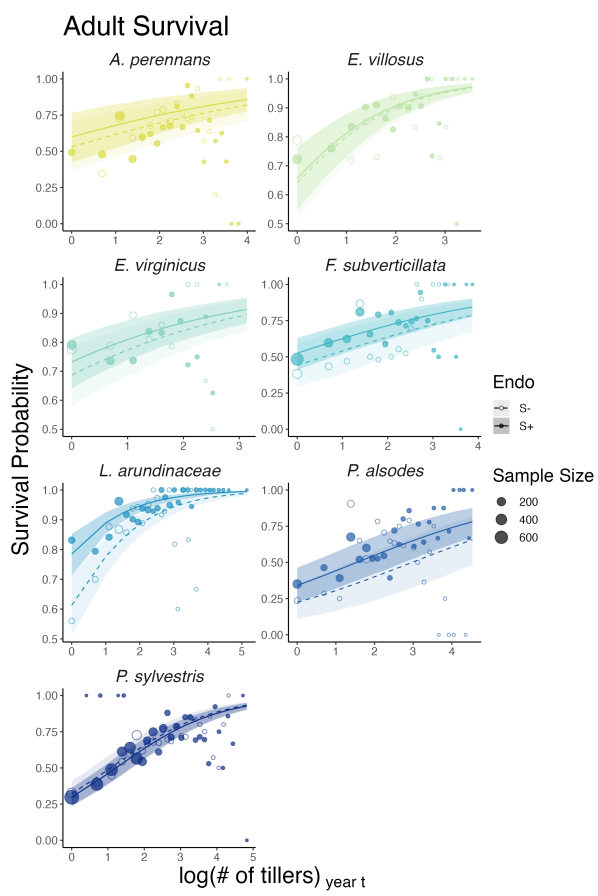
993

994

995

996

997



998 **Fig. S1** Effect of endophyte symbiosis on mean adult survival. Fitted curves represent the size-  
999 specific mean survival probability along with data binned by size shown as open circles with a dashed  
1000 line for symbiont-free (S-) plants, while the solid line and filled circles represent symbiotic (S+)  
1001 plants. 80% credible intervals are shown with dark shading for S+, or light shading for S-.

1002

1003

1004

1005

1006

1007

1008

1009

1010

1011

1012

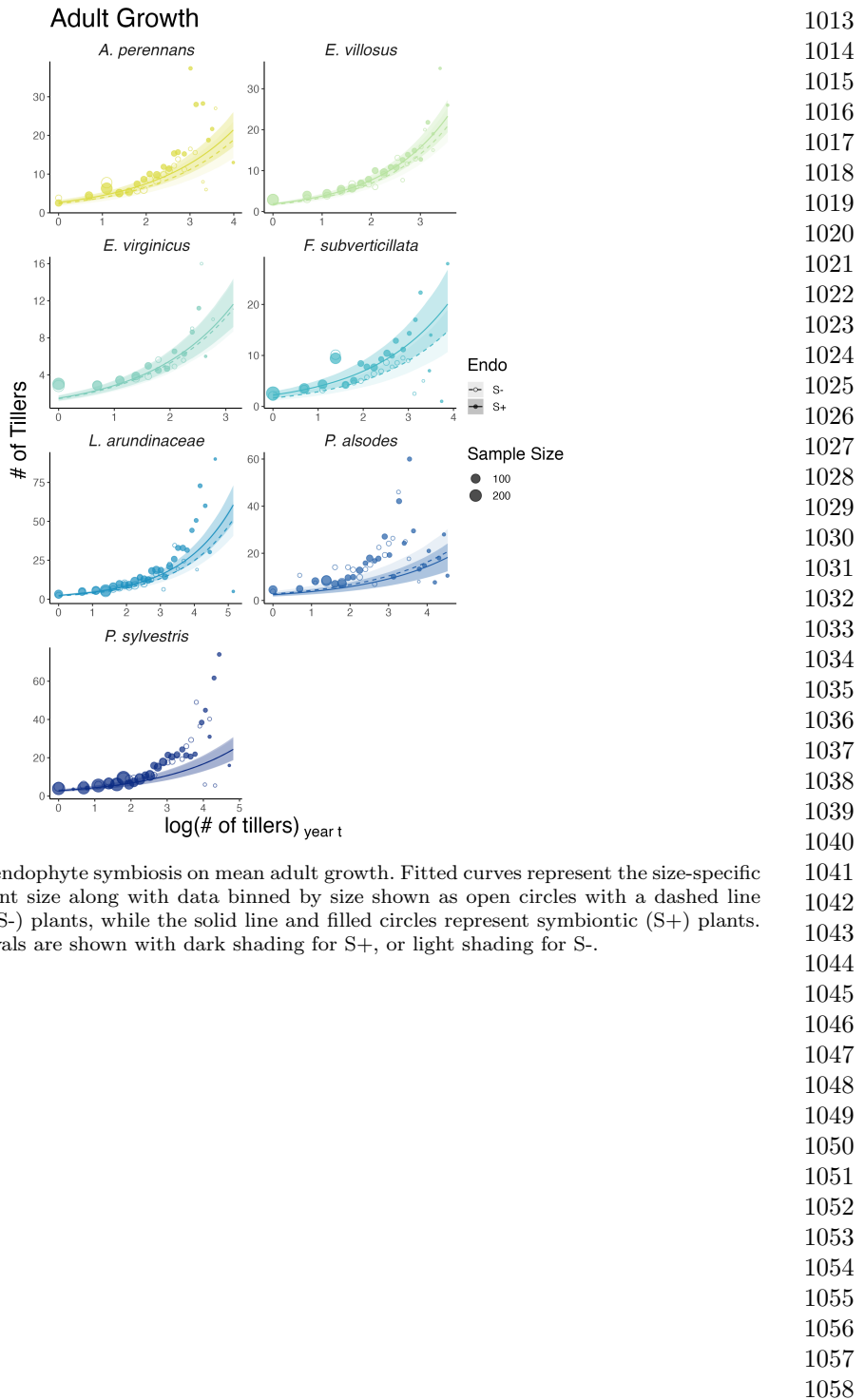
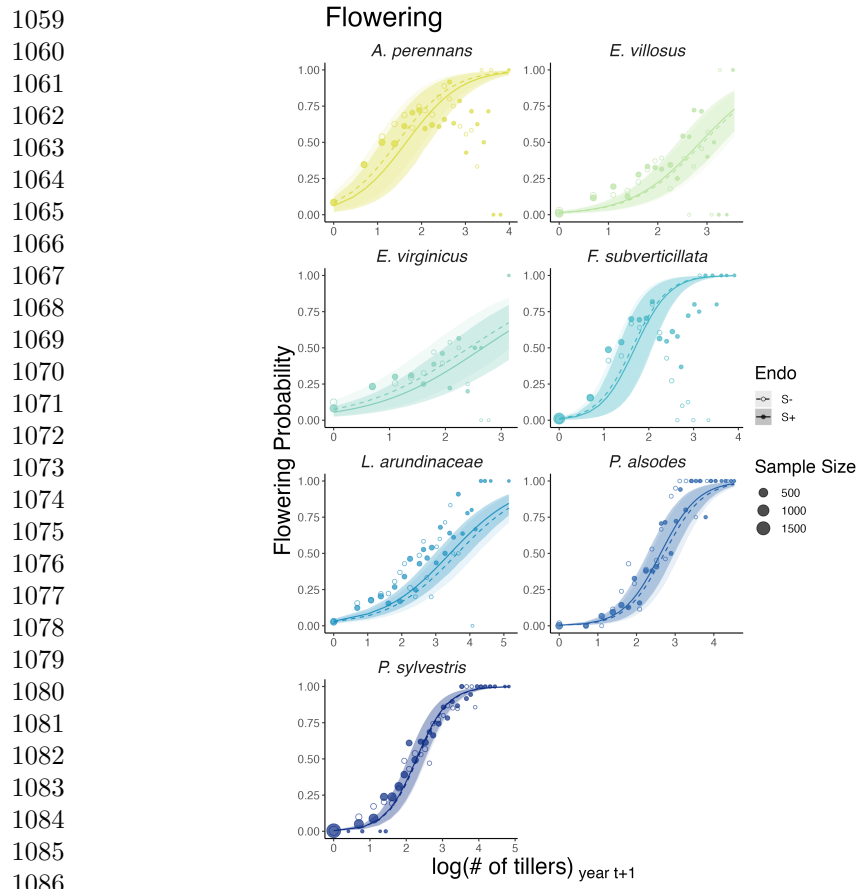


**Fig. S2** Effect of endophyte symbiosis on mean adult growth. Fitted curves represent the size-specific mean expected plant size along with data binned by size shown as open circles with a dashed line for symbiont-free (S-) plants, while the solid line and filled circles represent symbiotic (S+) plants. 80% credible intervals are shown with dark shading for S+, or light shading for S-.



1087 **Fig. S3** Effect of endophyte symbiosis on mean flowering. Fitted curves represent the size-specific  
1088 mean flowering probability along with data binned by size shown as open circles with a dashed line  
1089 for symbiont-free (S-) plants, while the solid line and filled circles represent symbiotic (S+) plants.  
1090 80% credible intervals are shown with dark shading for S+, or light shading for S-.

1091  
1092  
1093  
1094  
1095  
1096  
1097  
1098  
1099  
1100  
1101  
1102  
1103  
1104

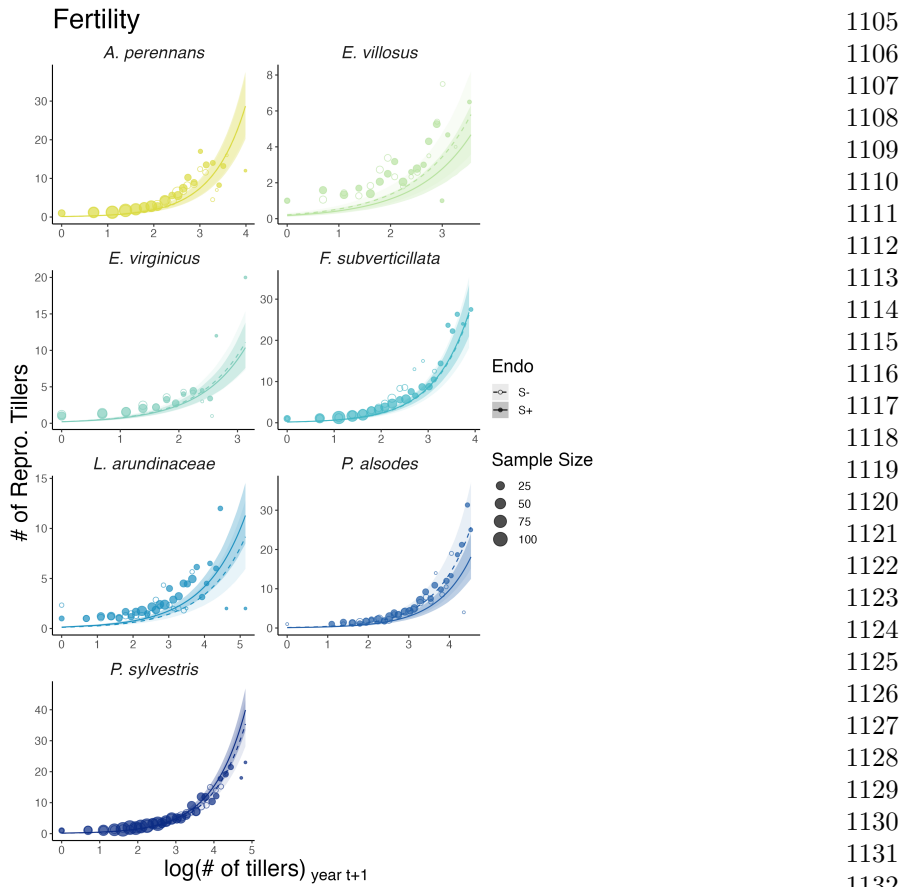
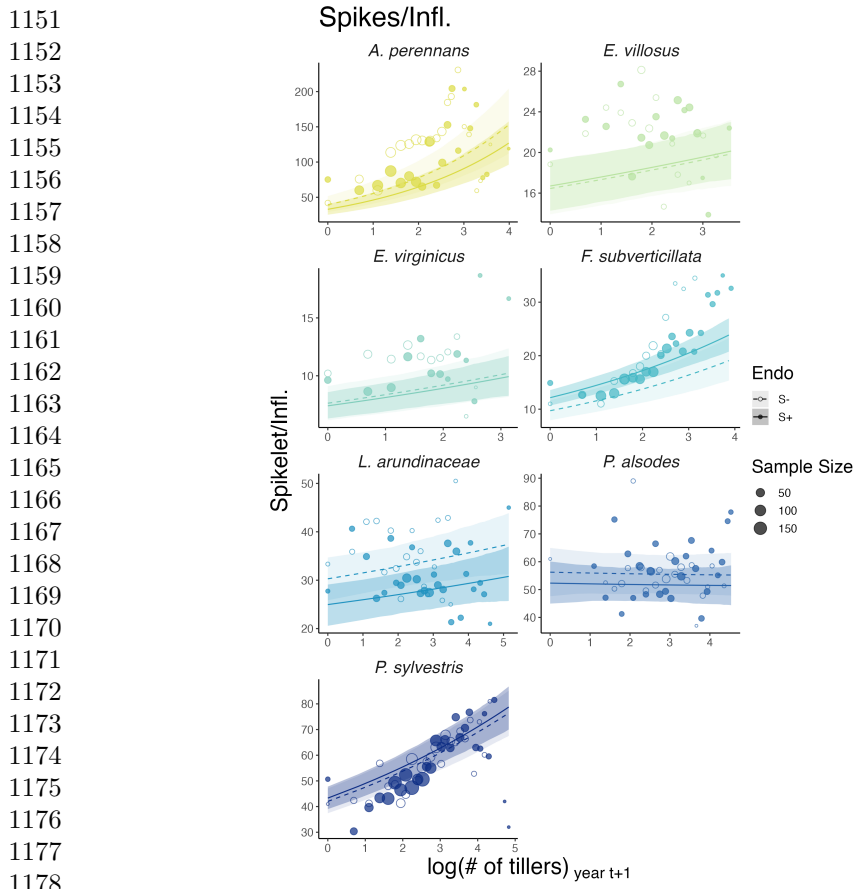


**Fig. S4** Effect of endophyte symbiosis on mean fertility. Fitted curves represent the size-specific mean expected number of flowering tillers along with data binned by size shown as open circles with a dashed line for symbiont-free (S-) plants, while the solid line and filled circles represent symbiotic (S+) plants. 80% credible intervals are shown with dark shading for S+, or light shading for S-.

1105  
1106  
1107  
1108  
1109  
1110  
1111  
1112  
1113  
1114  
1115  
1116  
1117  
1118  
1119  
1120  
1121  
1122  
1123  
1124  
1125  
1126  
1127  
1128  
1129  
1130  
1131  
1132  
1133  
1134  
1135  
1136  
1137  
1138  
1139  
1140  
1141  
1142  
1143  
1144  
1145  
1146  
1147  
1148  
1149  
1150



1179 **Fig. S5** Effect of endophyte symbiosis on mean spikelet production. Fitted curves represent the size-  
1180 specific mean expected number of spikelets per inflorescence along with data binned by size shown  
1181 as open circles with a dashed line for symbiont-free (S-) plants, while the solid line and filled circles  
1182 represent symbiotic (S+) plants. 80% credible intervals are shown with dark shading for S+, or light  
1183 shading for S-.

1183  
1184  
1185  
1186  
1187  
1188  
1189  
1190  
1191  
1192  
1193  
1194  
1195  
1196

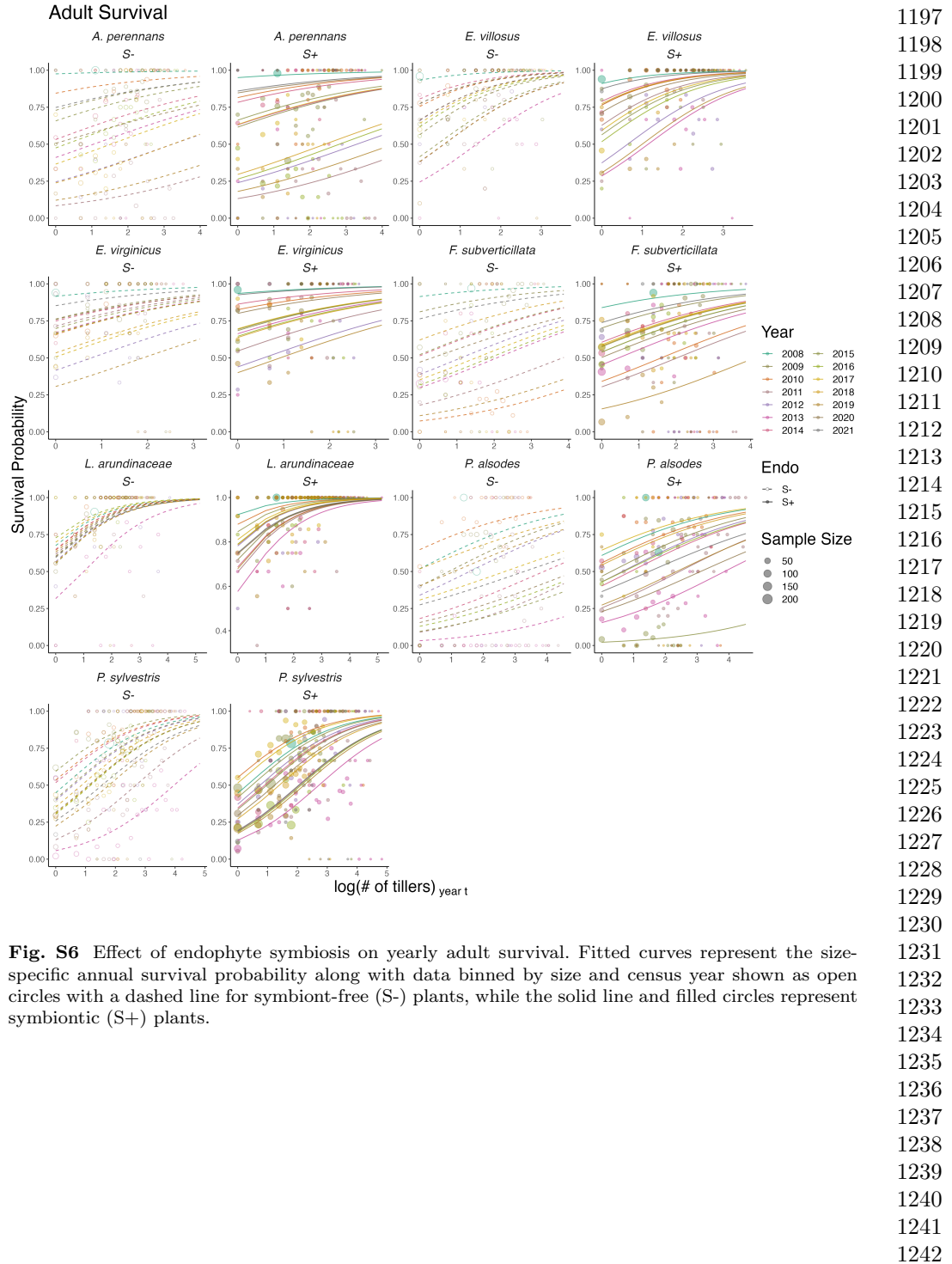
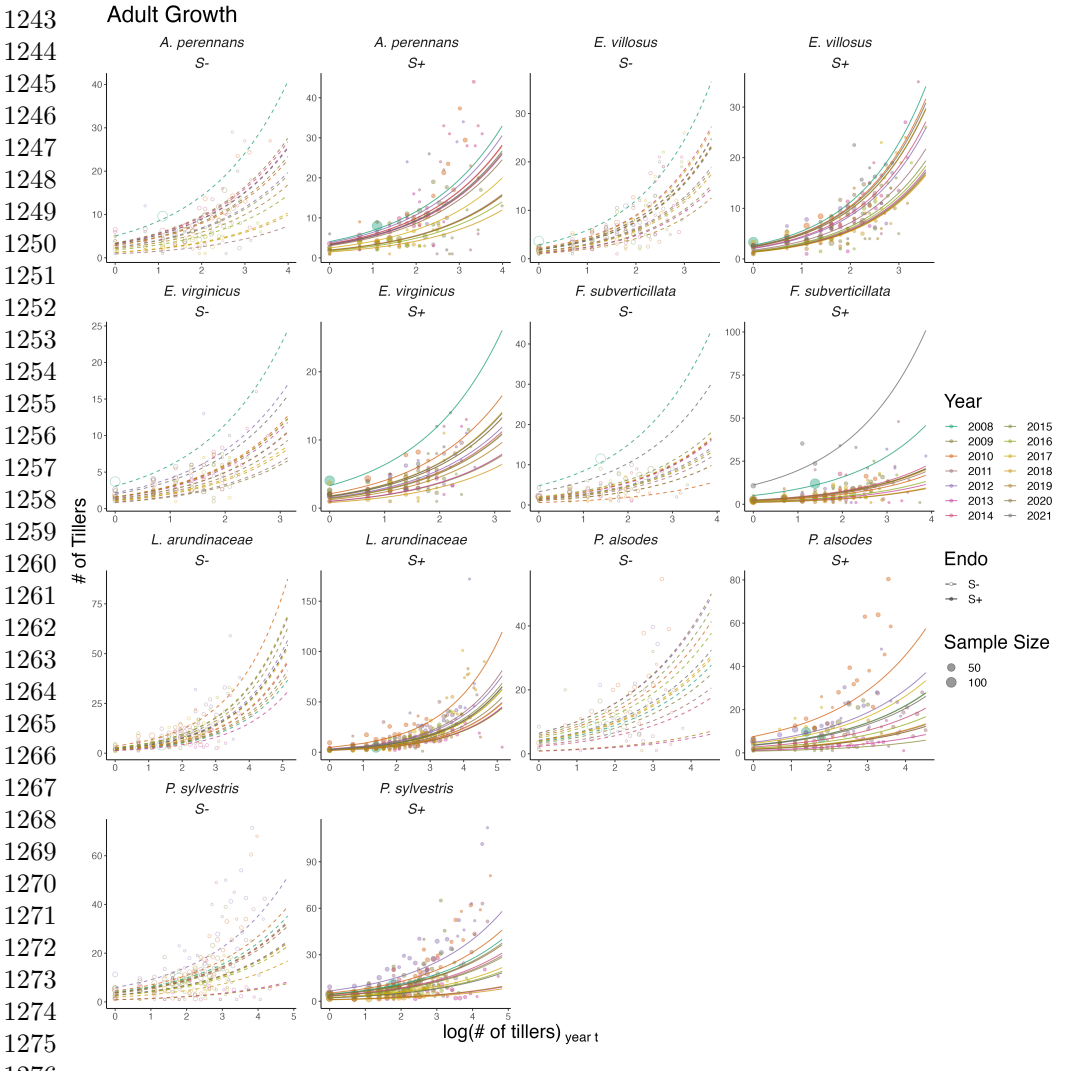


**Fig. S6** Effect of endophyte symbiosis on yearly adult survival. Fitted curves represent the size-specific annual survival probability along with data binned by size and census year shown as open circles with a dashed line for symbiont-free (S-) plants, while the solid line and filled circles represent symbiotic (S+) plants.



1277 **Fig. S7** Effect of endophyte symbiosis on yearly adult growth. Fitted curves represent the size-  
 1278 specific annual expected plant size along with data binned by size and census year shown as open  
 1279 circles with a dashed line for symbiont-free (S-) plants, while the solid line and filled circles represent  
 1280 symbiotic (S+) plants.

1281  
 1282  
 1283  
 1284  
 1285  
 1286  
 1287  
 1288

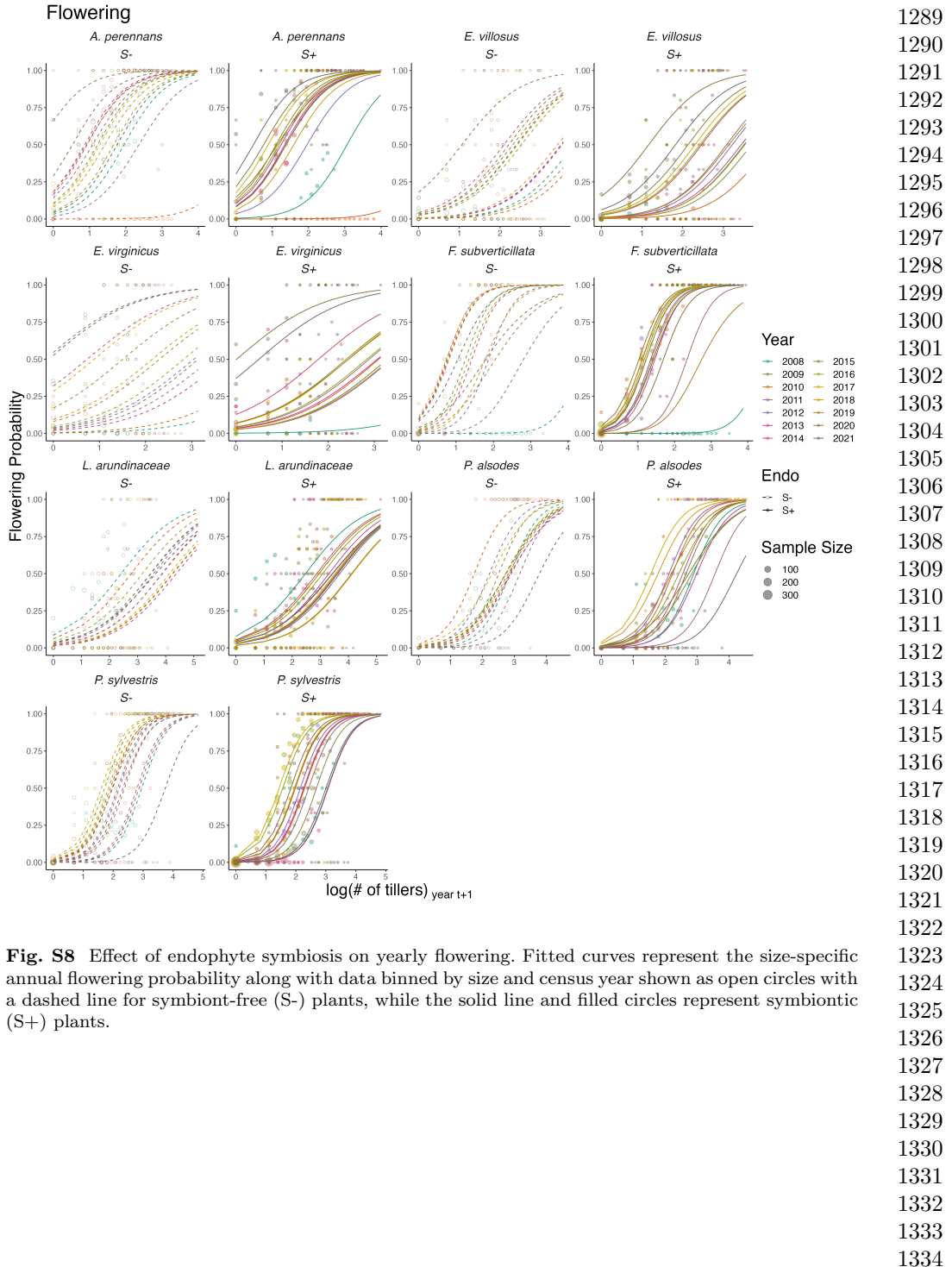
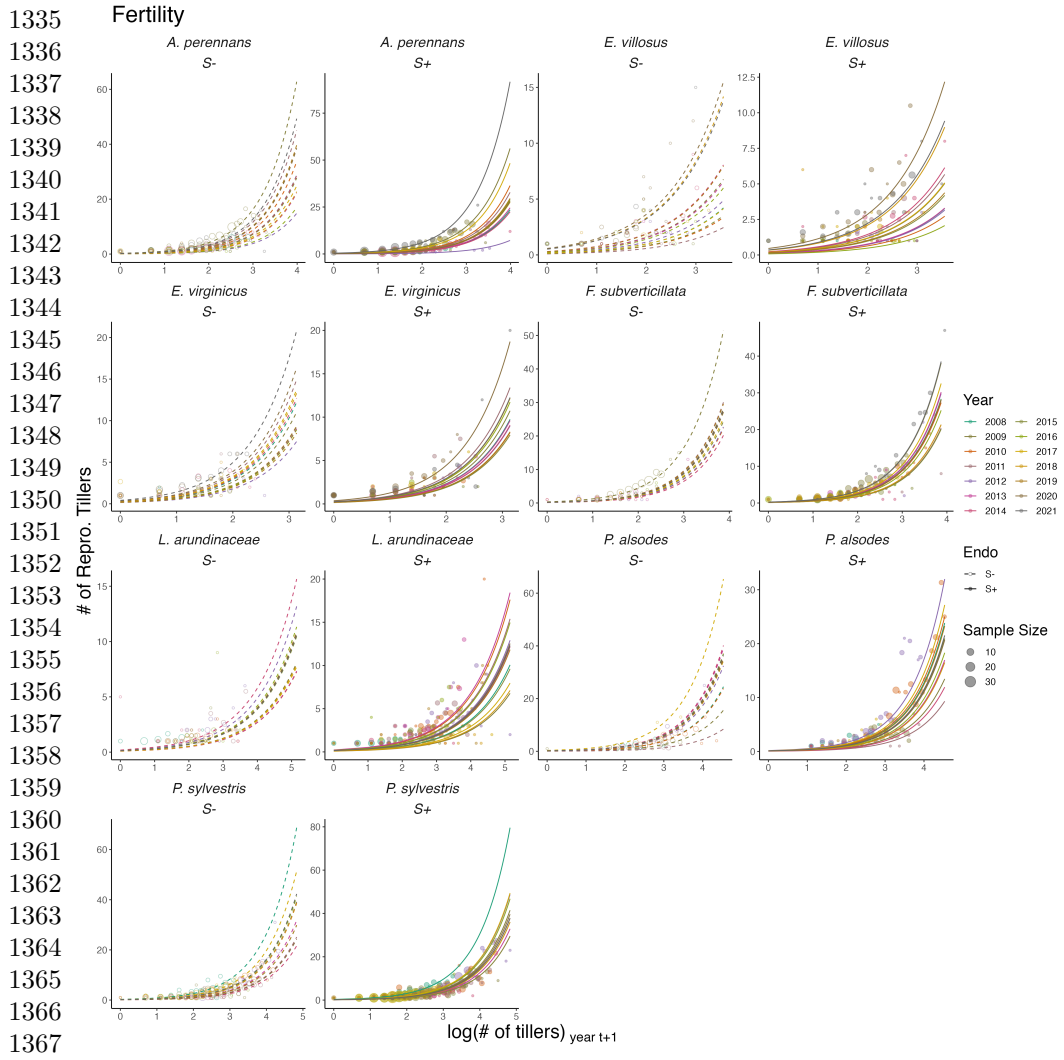


**Fig. S8** Effect of endophyte symbiosis on yearly flowering. Fitted curves represent the size-specific annual flowering probability along with data binned by size and census year shown as open circles with a dashed line for symbiont-free (S-) plants, while the solid line and filled circles represent symbiotic (S+) plants.



1369 **Fig. S9** Effect of endophyte symbiosis on yearly fertility. Fitted curves represent the size-specific  
 1370 annual expected number of flowering tillers along with data binned by size and census year shown  
 1371 as open circles with a dashed line for symbiont-free (S-) plants, while the solid line and filled circles  
 1372 represent symbiotic (S+) plants.

1372  
 1373  
 1374  
 1375  
 1376  
 1377  
 1378  
 1379  
 1380

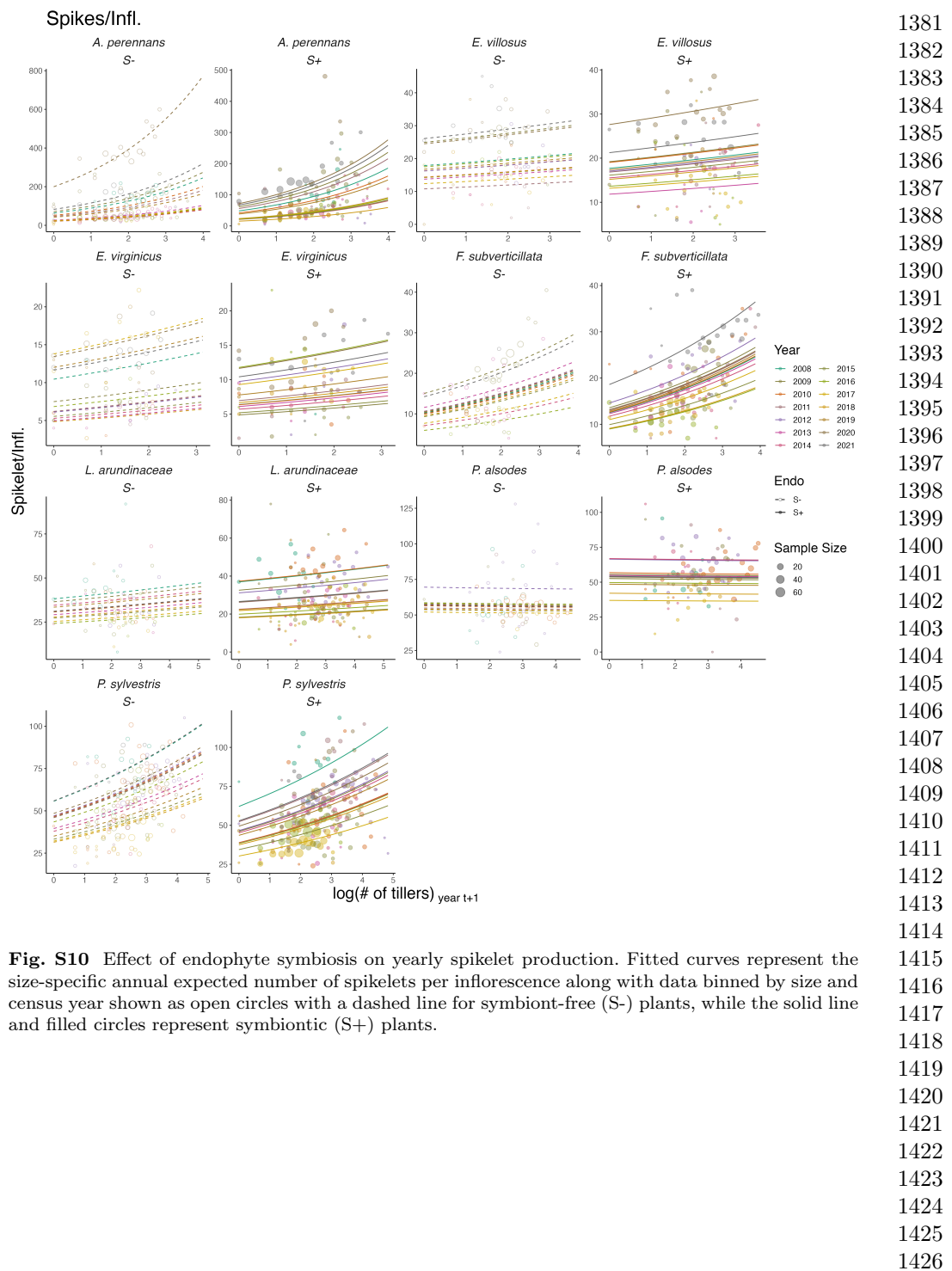
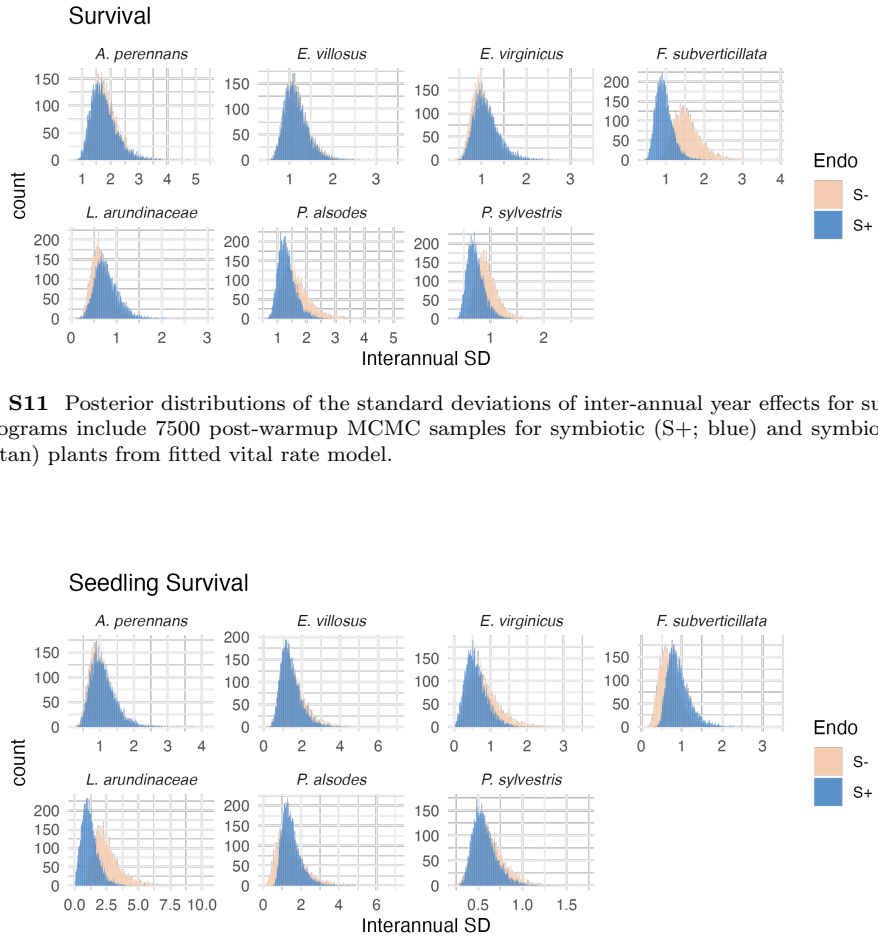


**Fig. S10** Effect of endophyte symbiosis on yearly spikelet production. Fitted curves represent the size-specific annual expected number of spikelets per inflorescence along with data binned by size and census year shown as open circles with a dashed line for symbiont-free (S-) plants, while the solid line and filled circles represent symbiotic (S+) plants.



1439 **Fig. S11** Posterior distributions of the standard deviations of inter-annual year effects for survival.  
 1440 Histograms include 7500 post-warmup MCMC samples for symbiotic (S+; blue) and symbiont-free  
 1441 (S-; tan) plants from fitted vital rate model.

Figure 2 consists of seven histograms arranged in two rows. The top row contains four histograms for *A. perennans*, *E. villosus*, *E. virginicus*, and *F. subverticillata*. The bottom row contains three histograms for *L. arundinaceae*, *P. alsodes*, and *P. sylvestris*. The y-axis for all histograms is 'Count' ranging from 0 to 150. The x-axis is 'Interannual SD' with varying scales: *A. perennans* (0-4), *E. villosus* (0-6), *E. virginicus* (0-3), *F. subverticillata* (0-3), *L. arundinaceae* (0.0-10.0), *P. alsodes* (0-6), and *P. sylvestris* (0-1.5). Each histogram features a blue shaded area representing 'S+' and an orange shaded area representing 'Endo'.

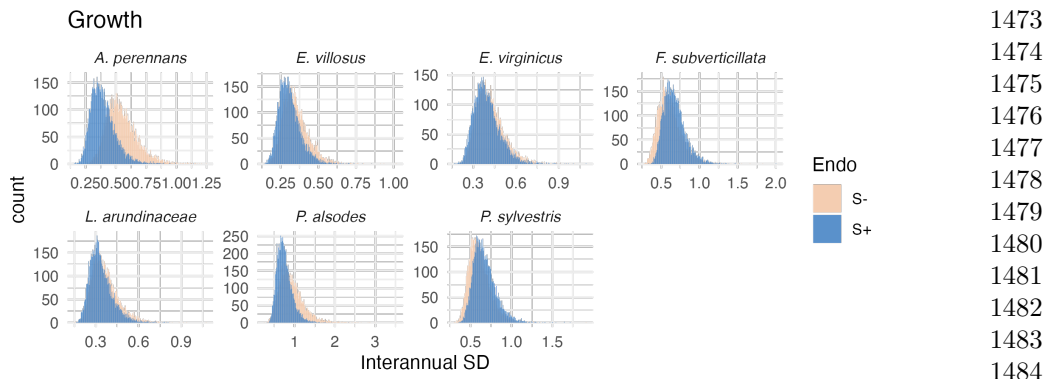


**Fig. S13** Posterior distributions of the standard deviations of inter-annual year effects for growth. Histograms include 7500 post-warmup MCMC samples for symbiotic (S+; blue) and symbiont-free (S-; tan) plants from fitted vital rate model.

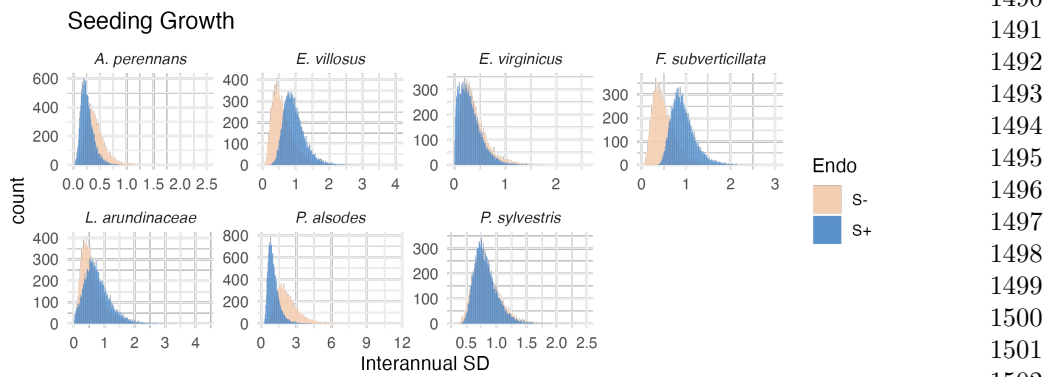
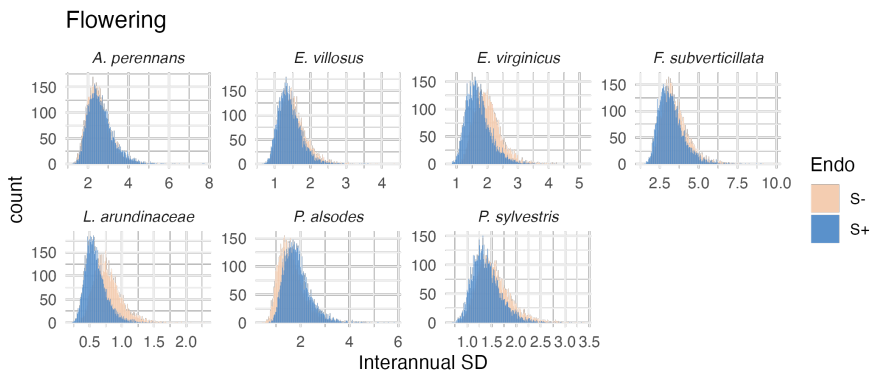


**Fig. S14** Posterior distributions of the standard deviations of inter-annual year effects for seedling growth. Histograms include 7500 post-warmup MCMC samples for symbiotic (S+; blue) and symbiont-free (S-; tan) plants from fitted vital rate model.

1473  
1474  
1475  
1476  
1477  
1478  
1479  
1480  
1481  
1482  
1483  
1484  
1485  
1486  
1487  
1488  
1489  
1490  
1491  
1492  
1493  
1494  
1495  
1496  
1497  
1498  
1499  
1500  
1501  
1502  
1503  
1504  
1505  
1506  
1507  
1508  
1509  
1510  
1511  
1512  
1513  
1514  
1515  
1516  
1517  
1518

1519



1531 **Fig. S15** Posterior distributions of the standard deviations of inter-annual year effects for flowering  
 1532 probability. Histograms include 7500 post-warmup MCMC samples for symbiotic (S+; blue) and  
 1533 symbiont-free (S-; tan) plants from fitted vital rate model.

1534

1535

1536

1537

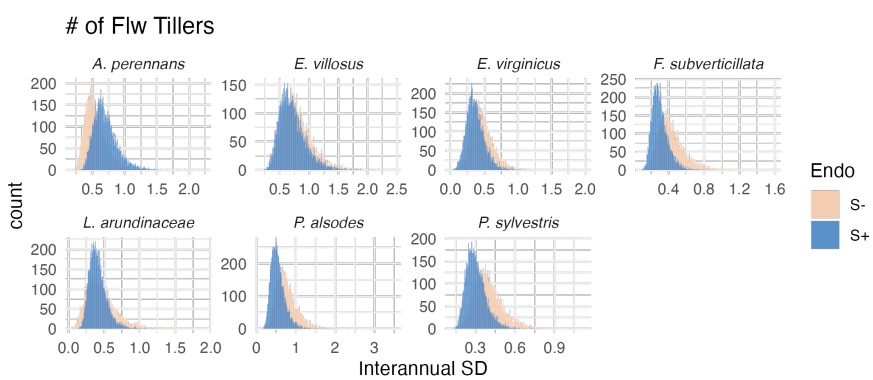


**Fig. S16** Posterior distributions of the standard deviations of inter-annual year effects for fertility (no. of flowering tillers). Histograms include 7500 post-warmup MCMC samples for symbiotic (S+; blue) and symbiont-free (S-; tan) plants from fitted vital rate model.

1551

1552

1553

1554

1555

1556

1557

1558

1559

1560

1561

1562

1563

1564

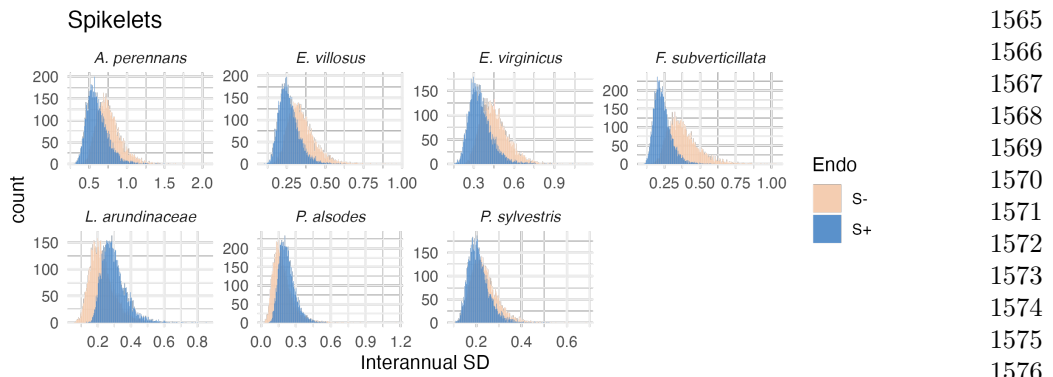


**Fig. S17** Posterior distributions of the standard deviations of inter-annual year effects for spikelets per inflorescence. Histograms include 7500 post-warmup MCMC samples for symbiotic (S+; blue) and symbiont-free (S-; tan) plants from fitted vital rate model.

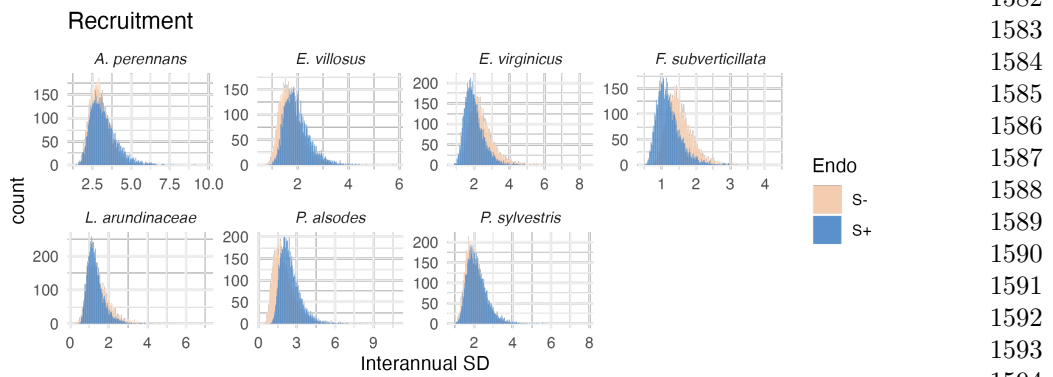
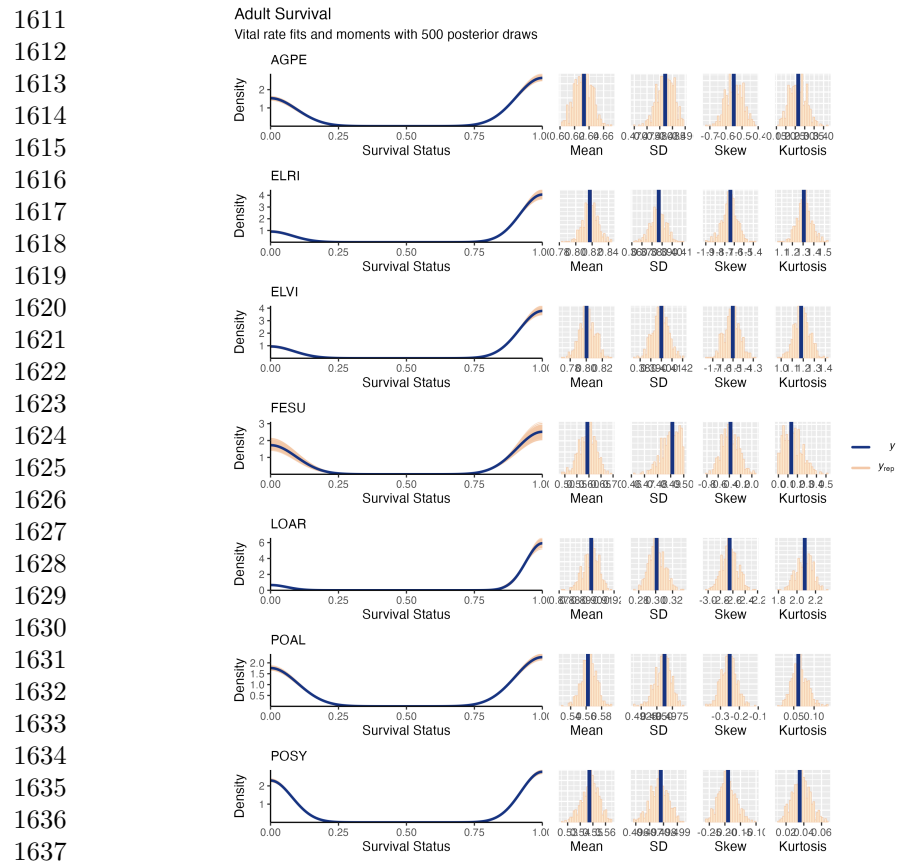


**Fig. S18** Posterior distributions of the standard deviations of inter-annual year effects for recruitment. Histograms include 7500 post-warmup MCMC samples for symbiotic (S+; blue) and symbiont-free (S-; tan) plants from fitted vital rate model.

1565  
1566  
1567  
1568  
1569  
1570  
1571  
1572  
1573  
1574  
1575  
1576  
1577  
1578  
1579  
1580  
1581  
1582  
1583  
1584  
1585  
1586  
1587  
1588  
1589  
1590  
1591  
1592  
1593  
1594  
1595  
1596  
1597  
1598  
1599  
1600  
1601  
1602  
1603  
1604  
1605  
1606  
1607  
1608  
1609  
1610



1638 **Fig. S19** Posterior predictive check for statistical model of Adult Survival. Consistency between  
1639 real data and simulated values indicates that fitted models describe the data well. Lines show den-  
1640 sity distributions of observed data (blue line) compared to data simulated from fitted models (tan  
1641 lines) generated from 500 draws from posterior distributions of model parameters along with the  
1642 distribution's moments.

1643  
1644  
1645  
1646  
1647  
1648  
1649  
1650  
1651  
1652  
1653  
1654  
1655  
1656

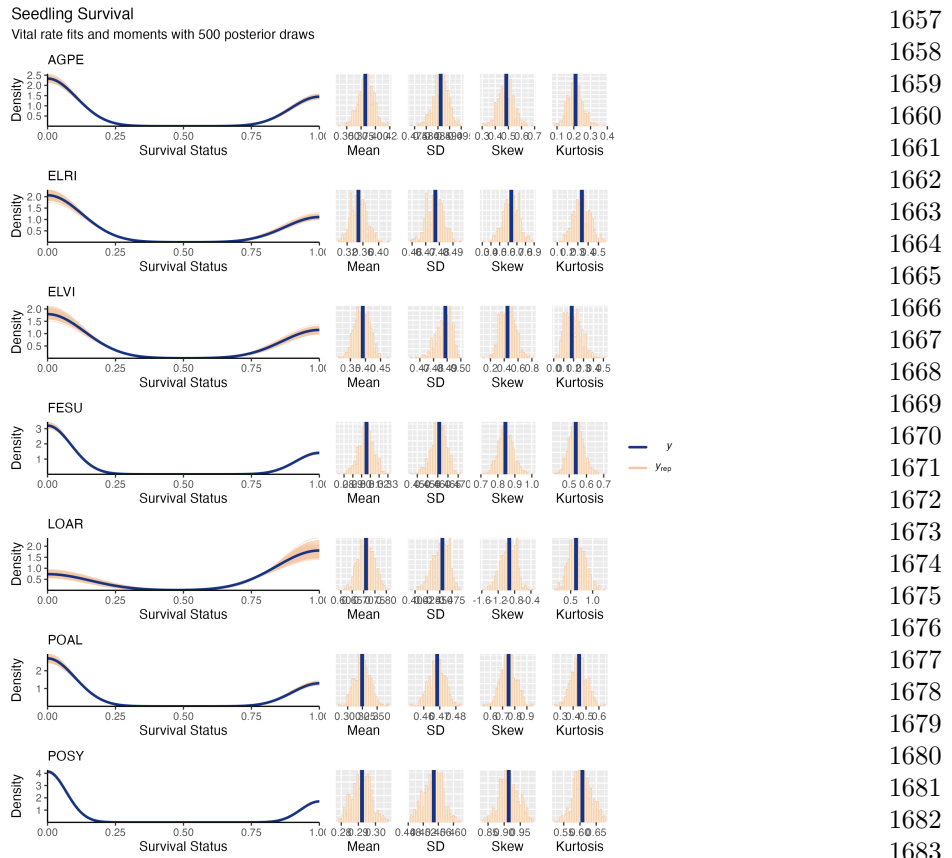


**Fig. S20** Posterior predictive check for statistical model of Seedling Survival. Consistency between real data and simulated values indicates that fitted models describe the data well. Lines show density distributions of observed data (blue line) compared to data simulated from fitted models (tan lines) generated from 500 draws from posterior distributions of model parameters along with the distribution's moments.

1657  
1658  
1659  
1660  
1661  
1662  
1663  
1664  
1665  
1666  
1667  
1668  
1669  
1670  
1671  
1672  
1673  
1674  
1675  
1676  
1677  
1678  
1679  
1680  
1681  
1682  
1683  
1684  
1685  
1686  
1687  
1688  
1689  
1690  
1691  
1692  
1693  
1694  
1695  
1696  
1697  
1698  
1699  
1700  
1701  
1702

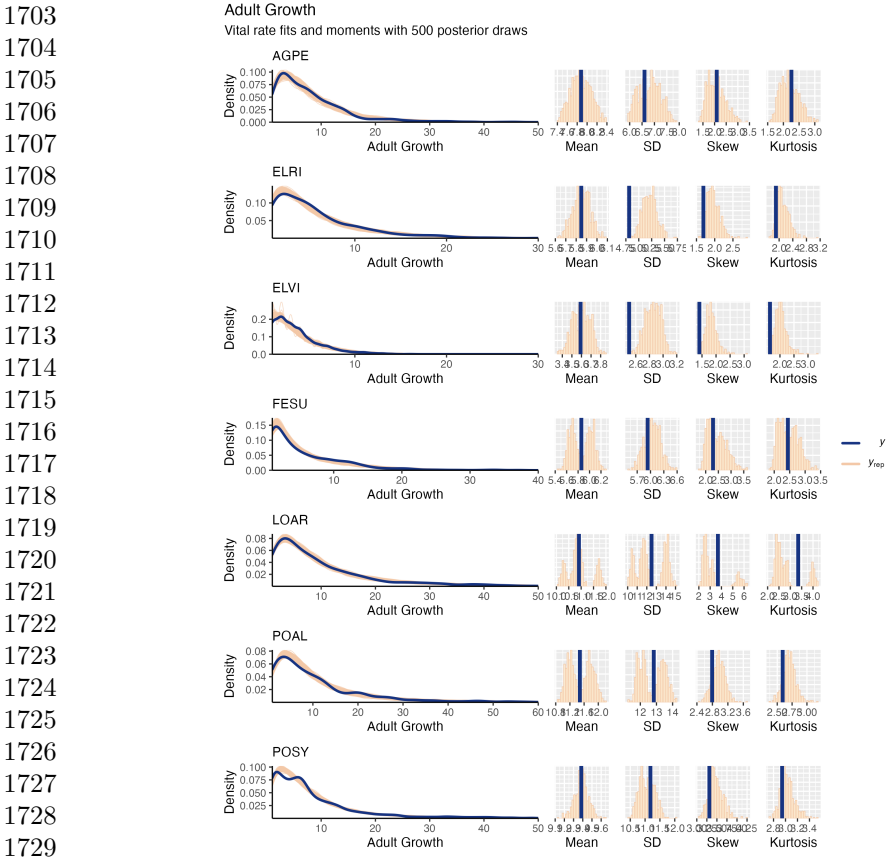


**Fig. S21** Posterior predictive check for statistical model of Adult Growth. Consistency between real data and simulated values indicates that fitted models describe the data well. Lines show density distributions of observed data (blue line) compared to data simulated from fitted models (tan lines) generated from 500 draws from posterior distributions of model parameters along with the distribution's moments.

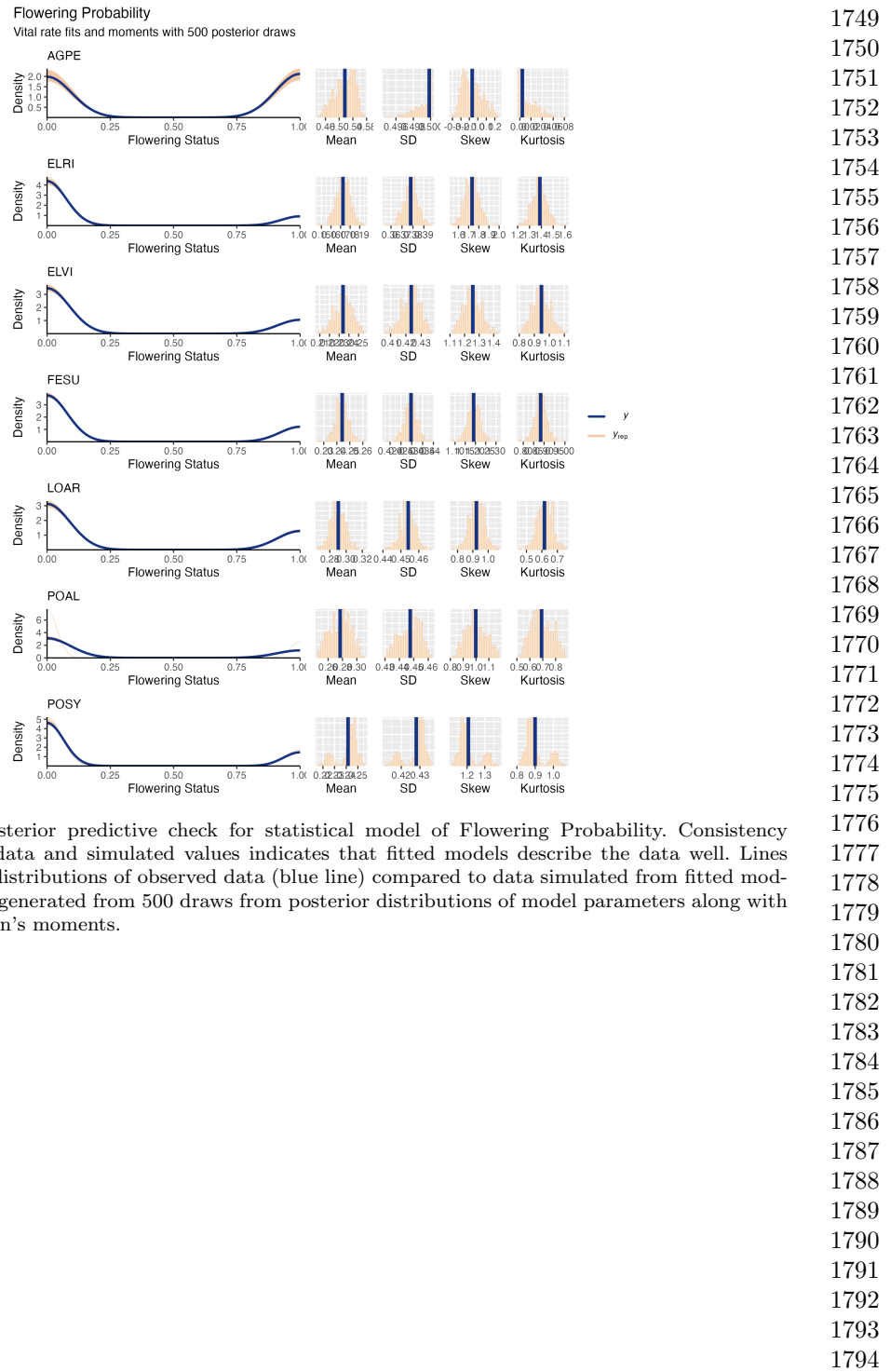
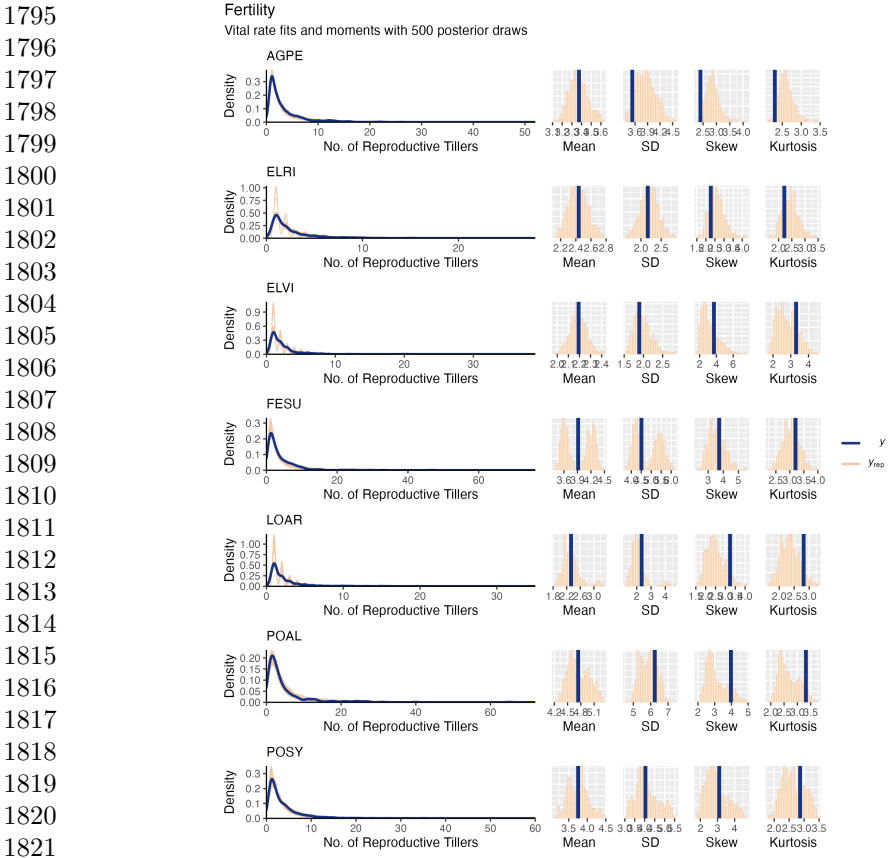
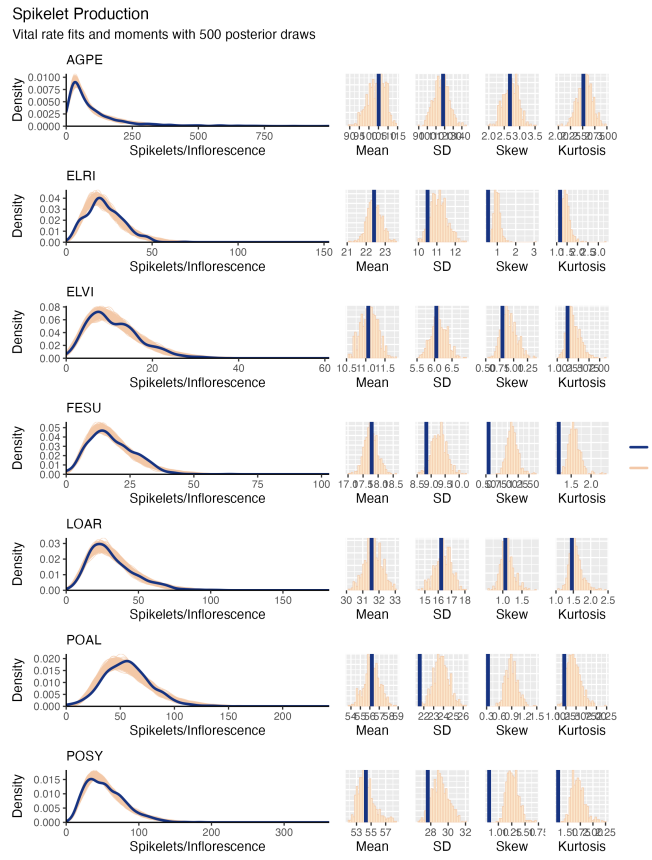


**Fig. S22** Posterior predictive check for statistical model of Flowering Probability. Consistency between real data and simulated values indicates that fitted models describe the data well. Lines show density distributions of observed data (blue line) compared to data simulated from fitted models (tan lines) generated from 500 draws from posterior distributions of model parameters along with the distribution's moments.



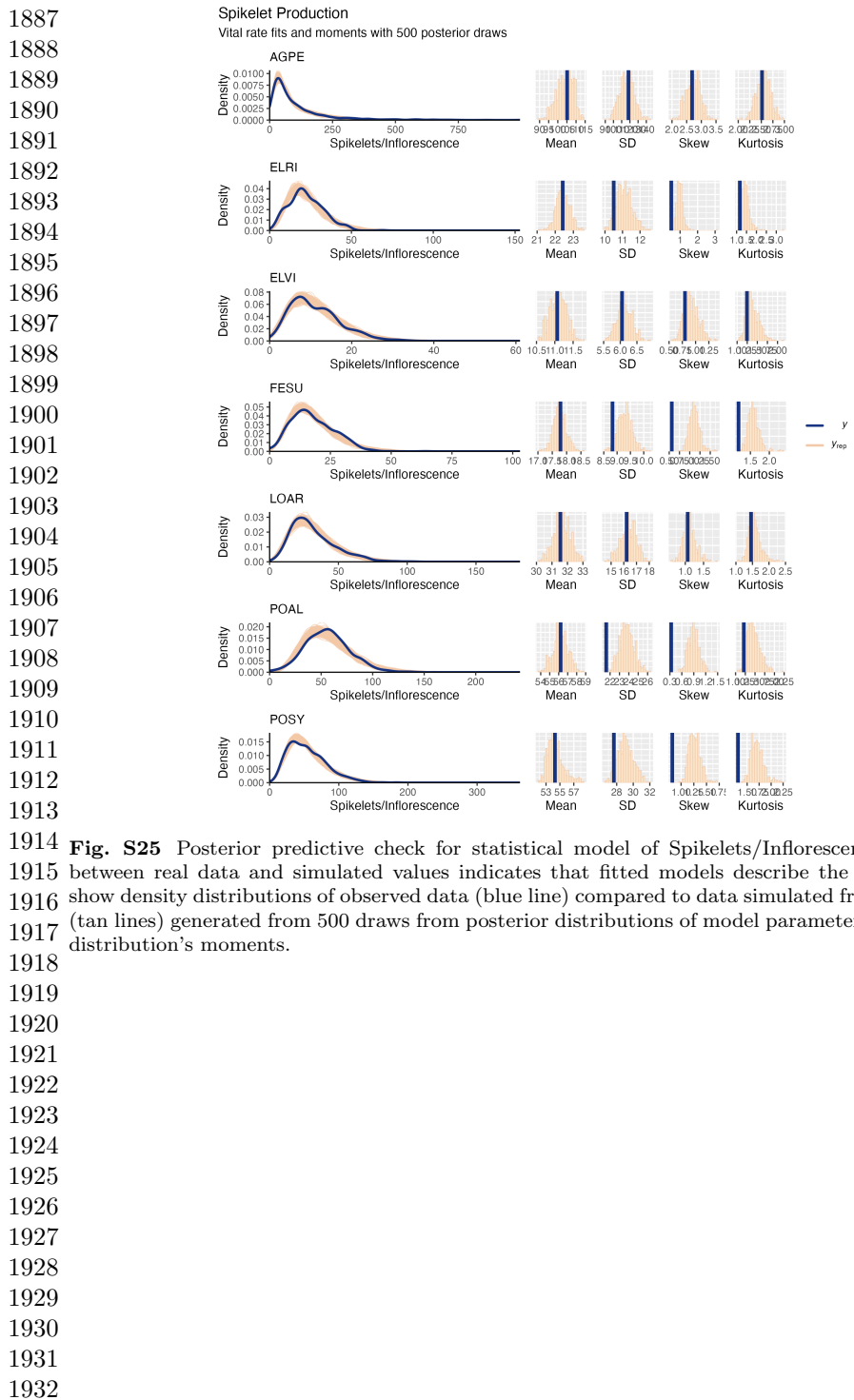
1822 **Fig. S23** Posterior predictive check for statistical model of Flowering Tiller Production. Consistency  
1823 between real data and simulated values indicates that fitted models describe the data well. Lines  
1824 show density distributions of observed data (blue line) compared to data simulated from fitted models  
1825 (tan lines) generated from 500 draws from posterior distributions of model parameters along with the  
1826 distribution's moments.

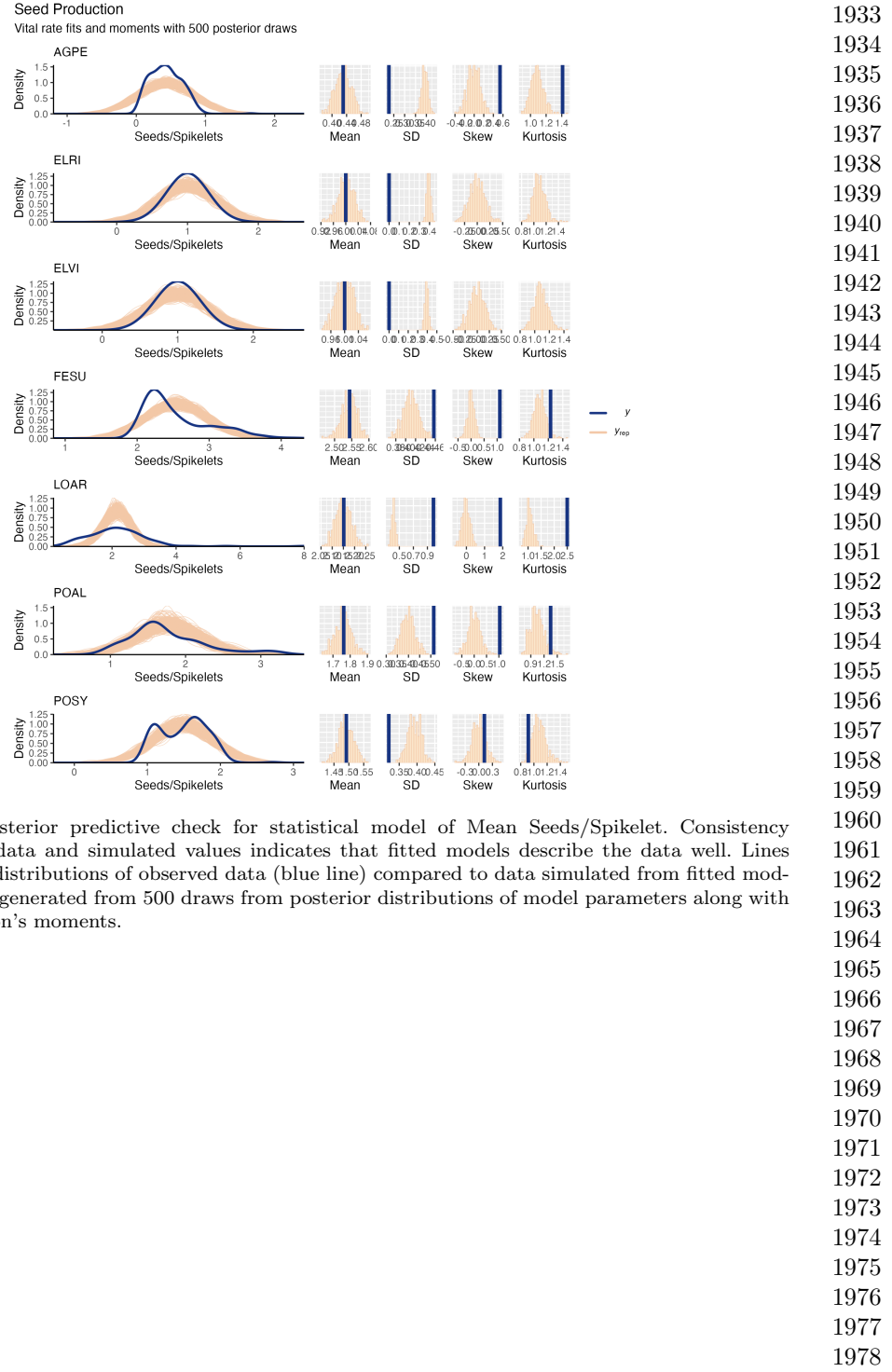
1826  
1827  
1828  
1829  
1830  
1831  
1832  
1833  
1834  
1835  
1836  
1837  
1838  
1839  
1840



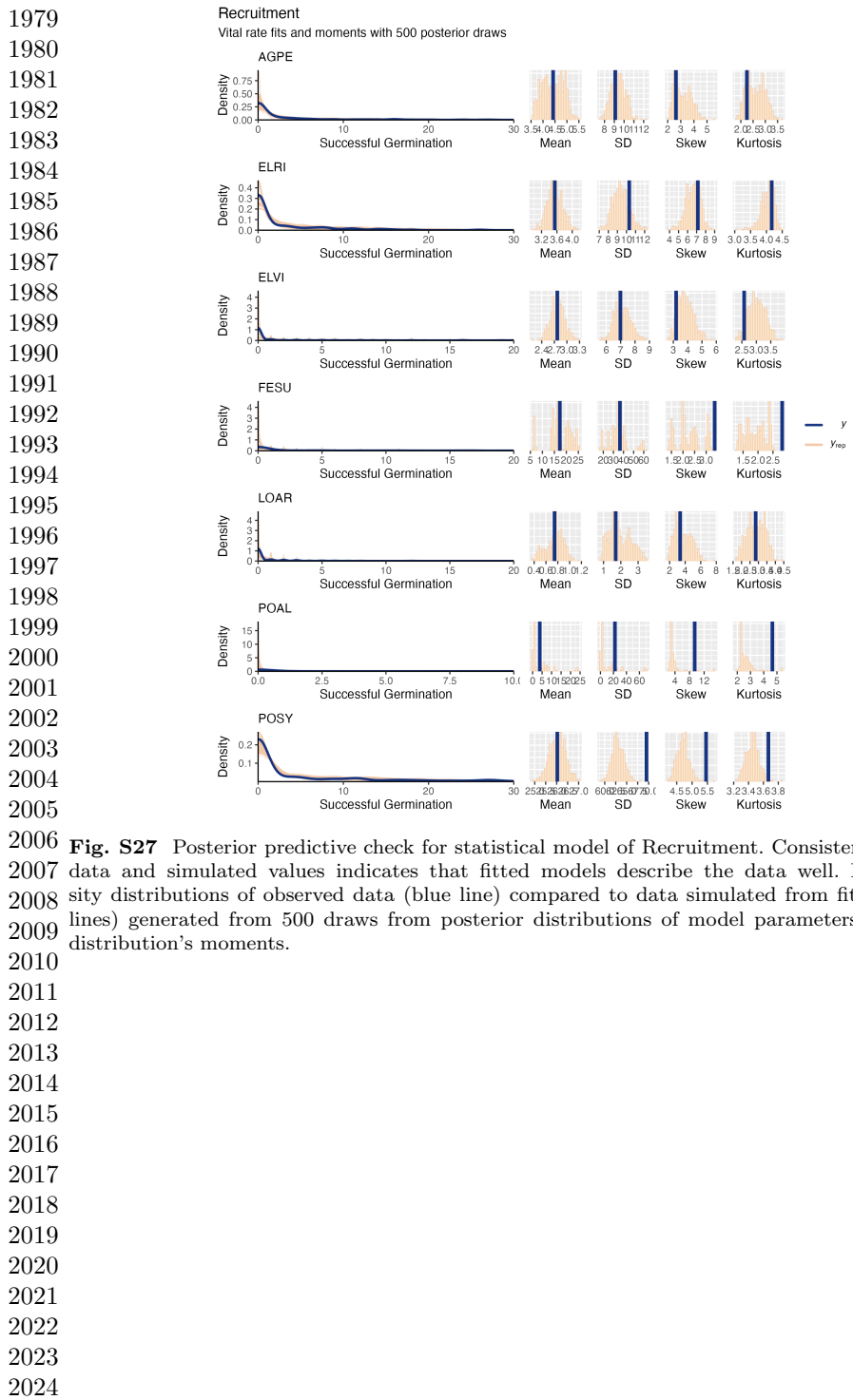
1841  
1842  
1843  
1844  
1845  
1846  
1847  
1848  
1849  
1850  
1851  
1852  
1853  
1854  
1855  
1856  
1857  
1858  
1859  
1860  
1861  
1862  
1863  
1864  
1865  
1866  
1867  
1868  
1869  
1870  
1871  
1872  
1873  
1874  
1875  
1876  
1877  
1878  
1879  
1880  
1881  
1882  
1883  
1884  
1885  
1886

**Fig. S24** Posterior predictive check for statistical model of Spikelets Production. Consistency between real data and simulated values indicates that fitted models describe the data well. Lines show density distributions of observed data (blue line) compared to data simulated from fitted models (tan lines) generated from 500 draws from posterior distributions of model parameters along with the distribution's moments.

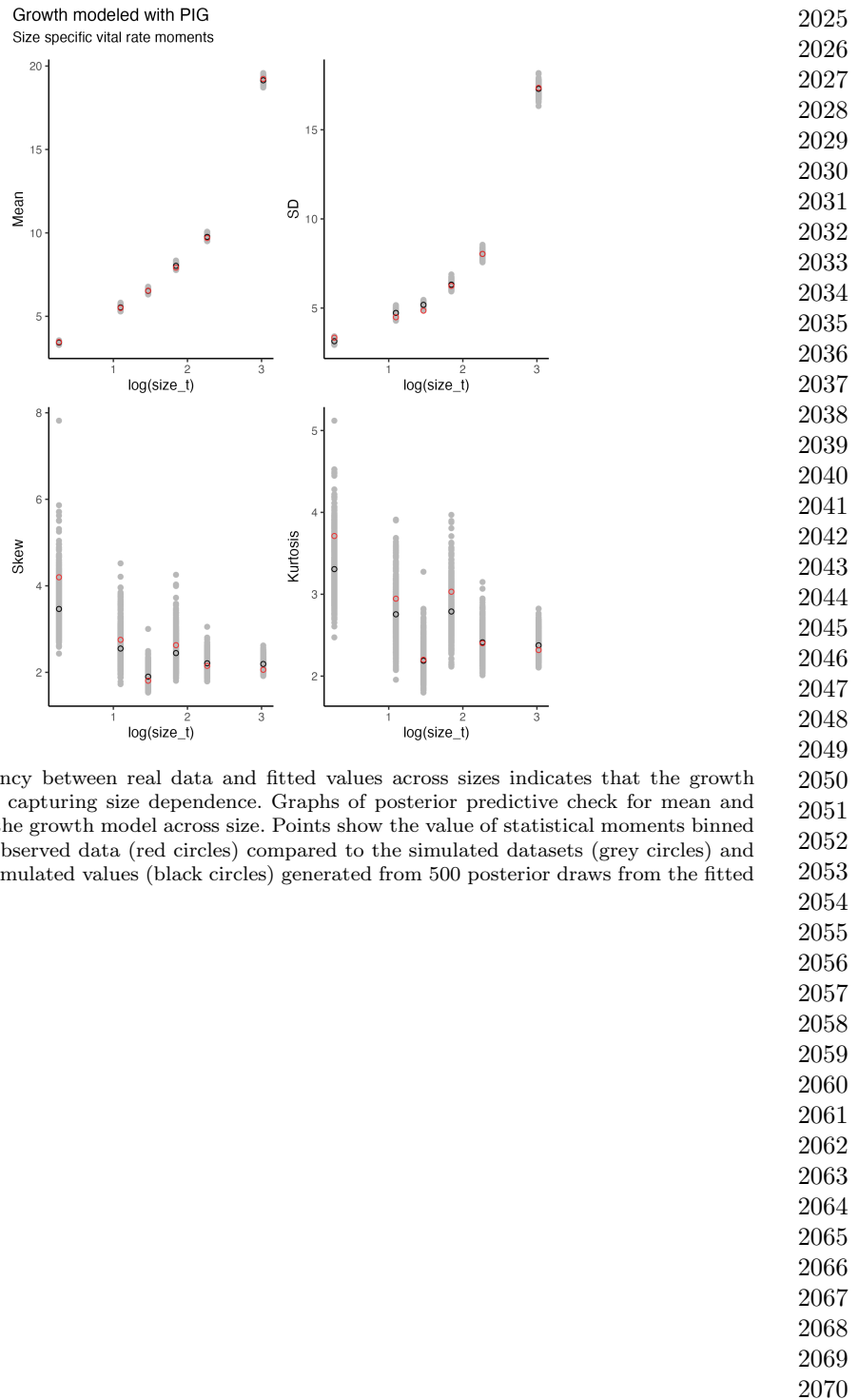




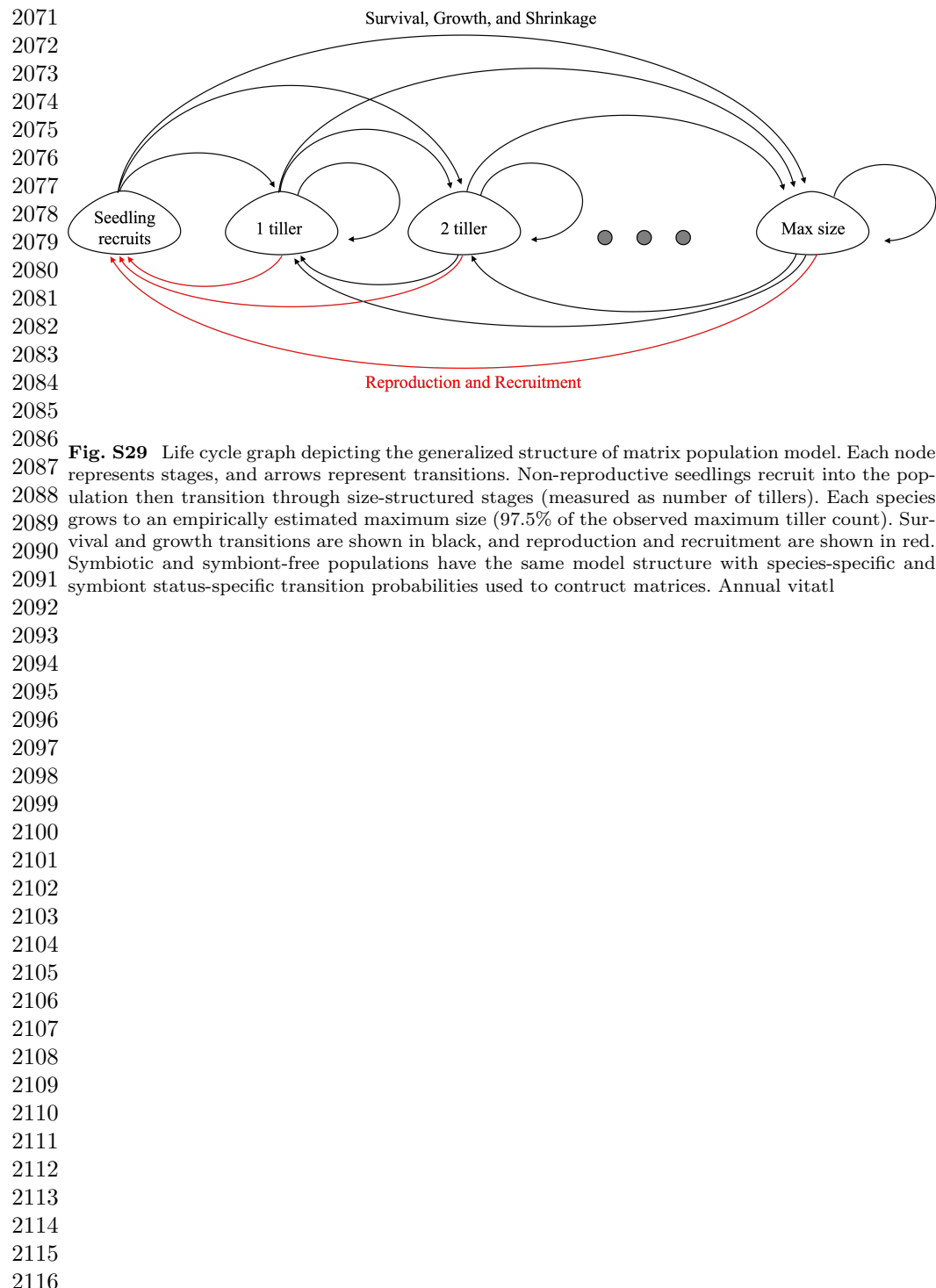
**Fig. S26** Posterior predictive check for statistical model of Mean Seeds/Spikelet. Consistency between real data and simulated values indicates that fitted models describe the data well. Lines show density distributions of observed data (blue line) compared to data simulated from fitted models (tan lines) generated from 500 draws from posterior distributions of model parameters along with the distribution's moments.

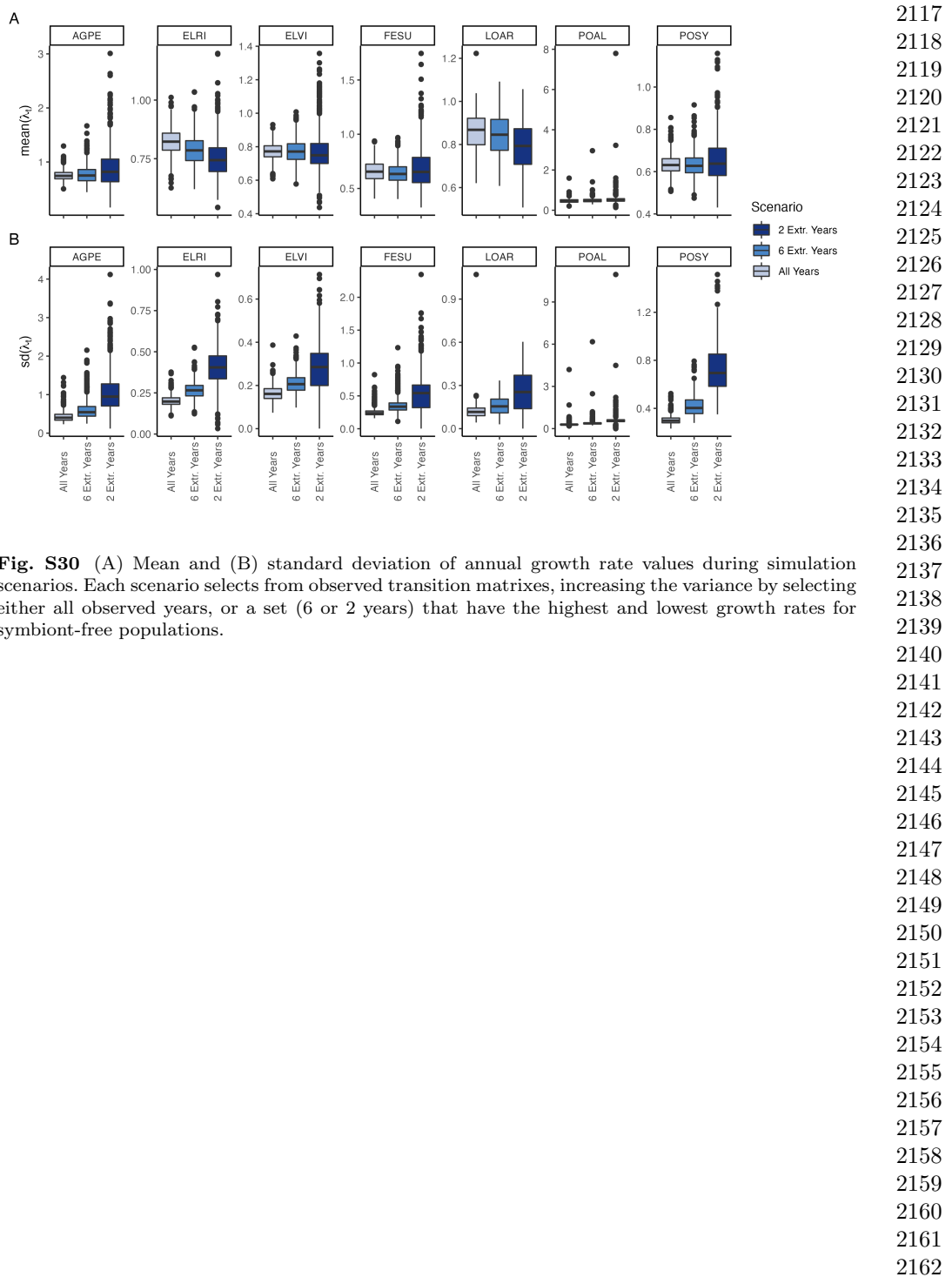


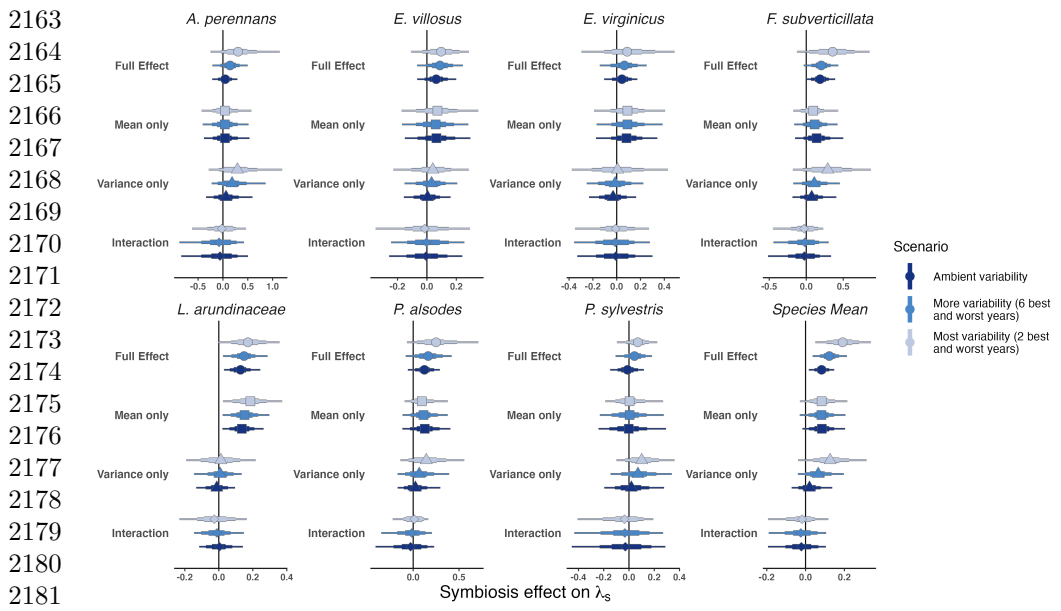
**Fig. S27** Posterior predictive check for statistical model of Recruitment. Consistency between real data and simulated values indicates that fitted models describe the data well. Lines show density distributions of observed data (blue line) compared to data simulated from fitted models (tan lines) generated from 500 draws from posterior distributions of model parameters along with the distribution's moments.



**Fig. S28** Consistency between real data and fitted values across sizes indicates that the growth model is accurately capturing size dependence. Graphs of posterior predictive check for mean and higher moments of the growth model across size. Points show the value of statistical moments binned across size for the observed data (red circles) compared to the simulated datasets (grey circles) and the median of the simulated values (black circles) generated from 500 posterior draws from the fitted model.







2183 **Fig. S31** Endophyte contributions to stochastic growth rates under observed and elevated variance  
2184 across species. The total effect of endophytes (circle) comes from mean benefits (square) and variance  
2185 buffering (triangle) as well as the interaction between mean and variance effects (diamond). Shapes  
2186 indicate the posterior mean of each contribution, along with bars for the 50, 75 and 95 % credible  
2187 intervals. Under scenarios of increasing variance, represented by increasing color intensity, effects of  
2188 variance buffering increase leading to a more mutualistic symbiosis.

2188  
2189  
2190  
2191  
2192  
2193  
2194  
2195  
2196  
2197  
2198  
2199  
2200  
2201  
2202  
2203  
2204  
2205  
2206  
2207  
2208

### Endophyte Status Checks

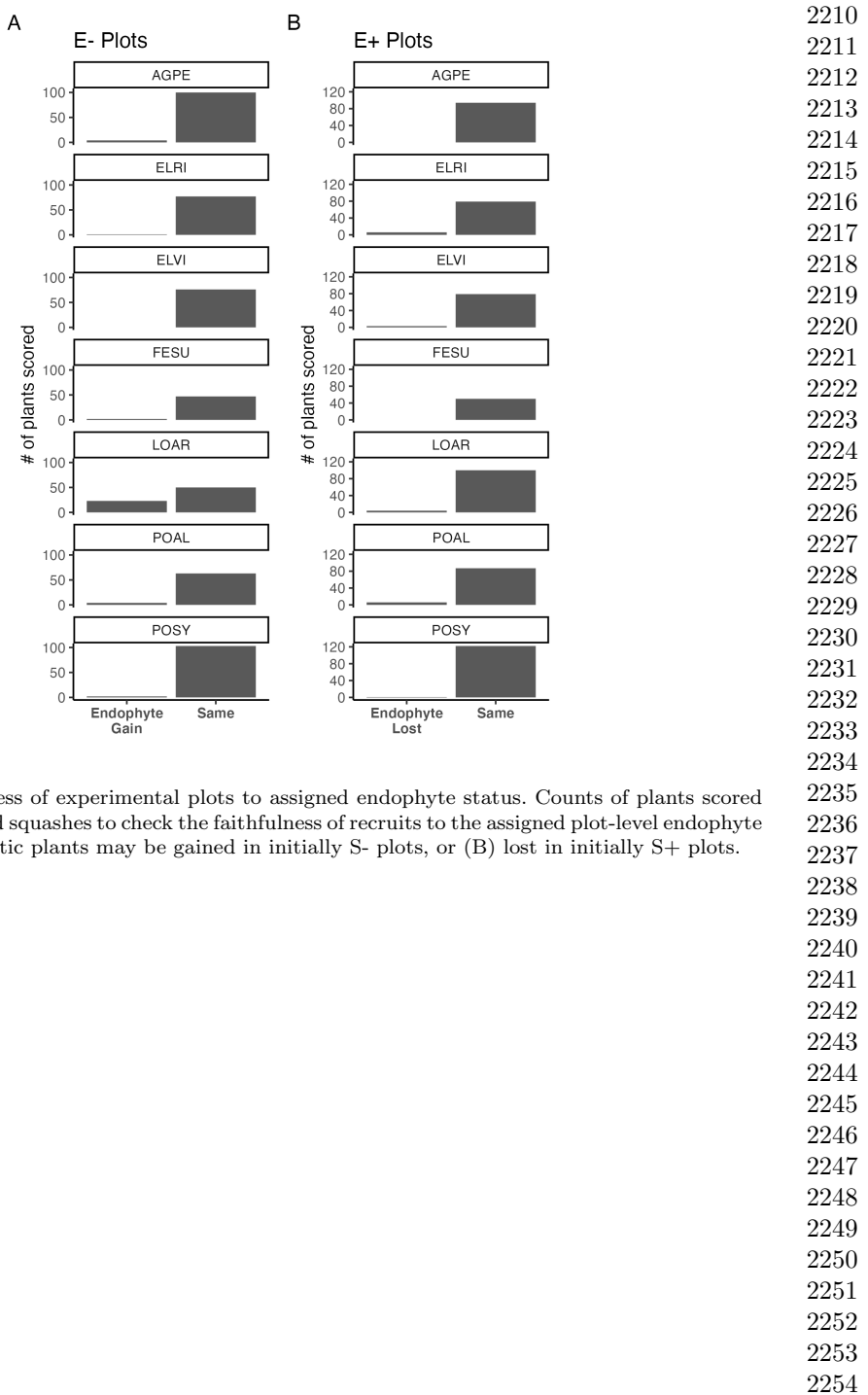
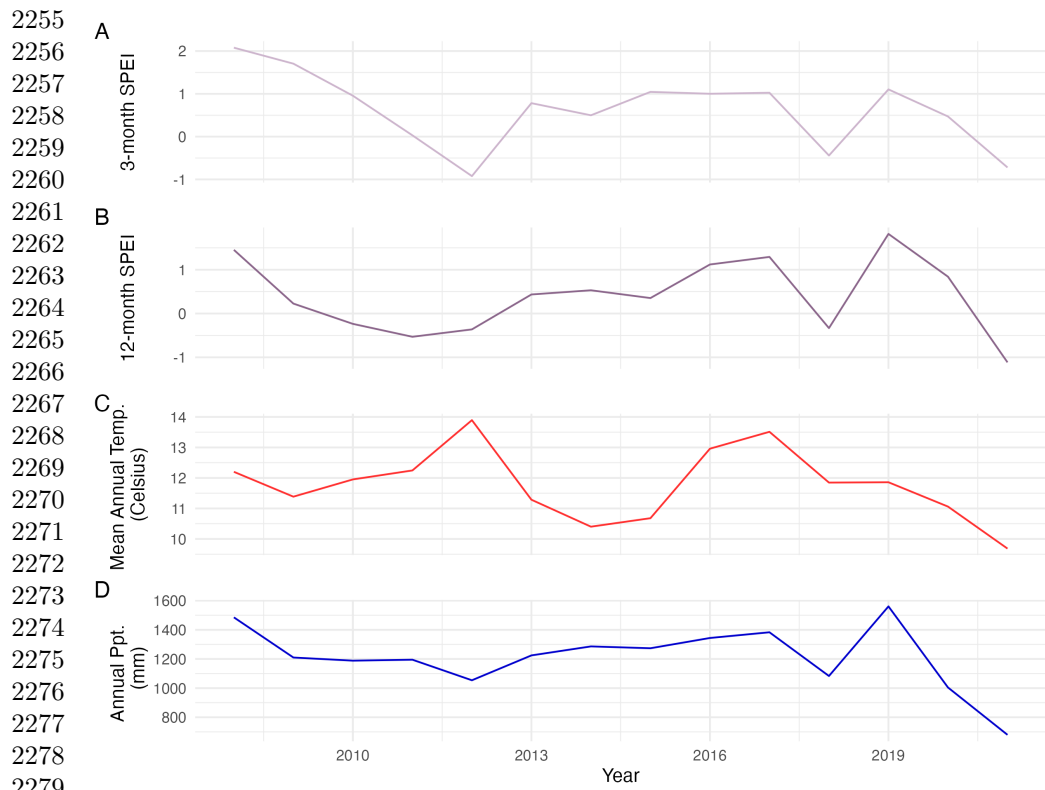


**Fig. S32** Faithfulness of experimental plots to assigned endophyte status. Counts of plants scored with leaf peels or seed squashes to check the faithfulness of recruits to the assigned plot-level endophyte status. (A) Endophytic plants may be gained in initially S- plots, or (B) lost in initially S+ plots.



2281 **Fig. S33** Weather station time-series for Bloomington, IN. The Seasonal Precipitation-  
 2282 Evapotranspiration Index (SPEI) calculated for the (A) three month growing season and (B) annually  
 2283 from daily weather station observations of (C) average temperatures and (D) cumulative precipitation.  
 2284 Climatic data shown are determined by the census year centered on the month of July.

2285  
 2286  
 2287  
 2288  
 2289  
 2290  
 2291  
 2292  
 2293  
 2294  
 2295  
 2296  
 2297  
 2298  
 2299  
 2300

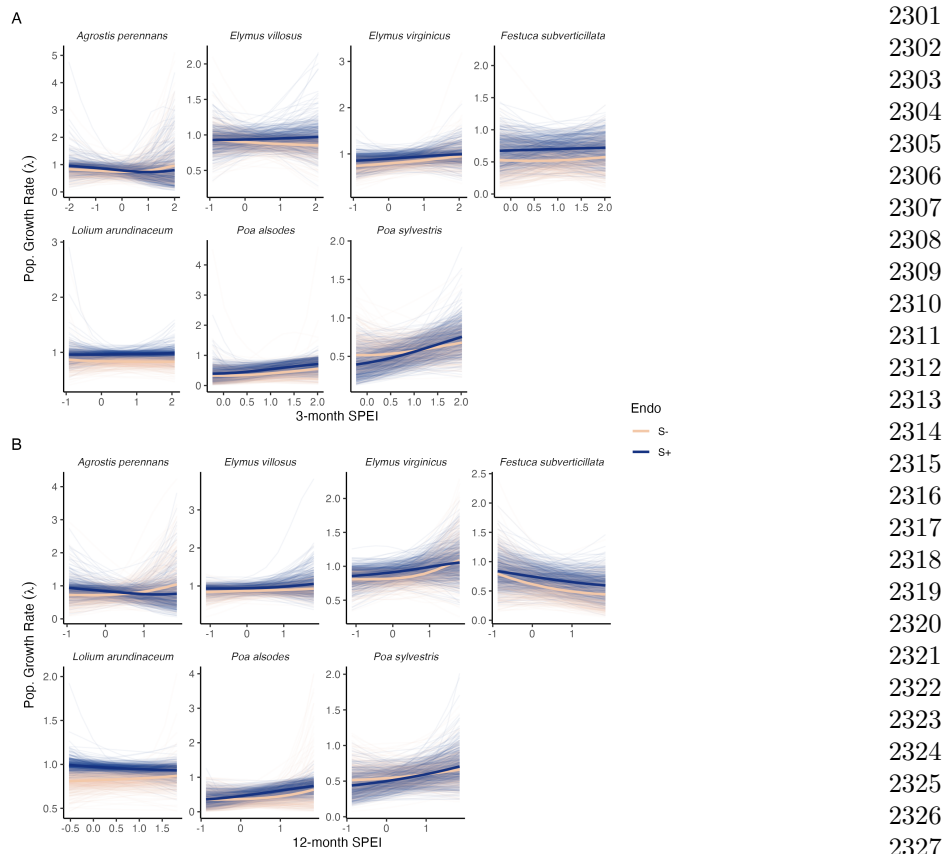


**Fig. S34** Predicted population growth rates across drought indices. Symbiotic (S+; blue) and symbiont-free (S-; tan) populations respond differently to climate as measured by the (A) 3-month SPEI and (B) 12-month SPEI. Thick lines represent the predicted mean growth rate and thin lines show 500 posterior draws.

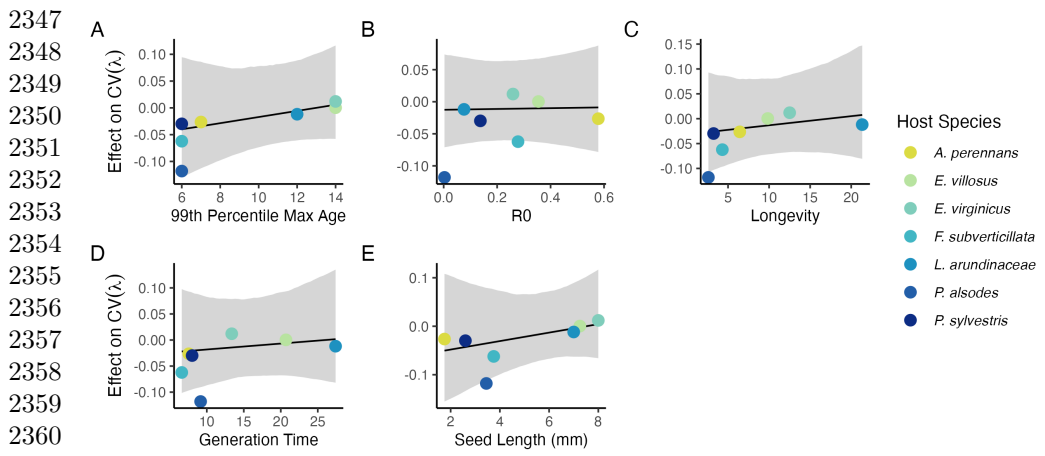


**Fig. S35** Relationship between variance buffering and life history traits describing the fast-slow life history continuum accounting for phylogenetic covariance between grass host species. Regressions between life history traits describing the fast-slow life history continuum ((A) 99th percentile maximum age observed during long term censuses in years; (B) Net reproductive rate; (C) Longevity; (D) Generation time in years; (E) Seed size) and the effect of endophyte symbiosis on the coefficient of variation in population growth rate ( $\lambda$ ). Each panel shows the fitted mean relationship (line) along with the 95% credible interval.

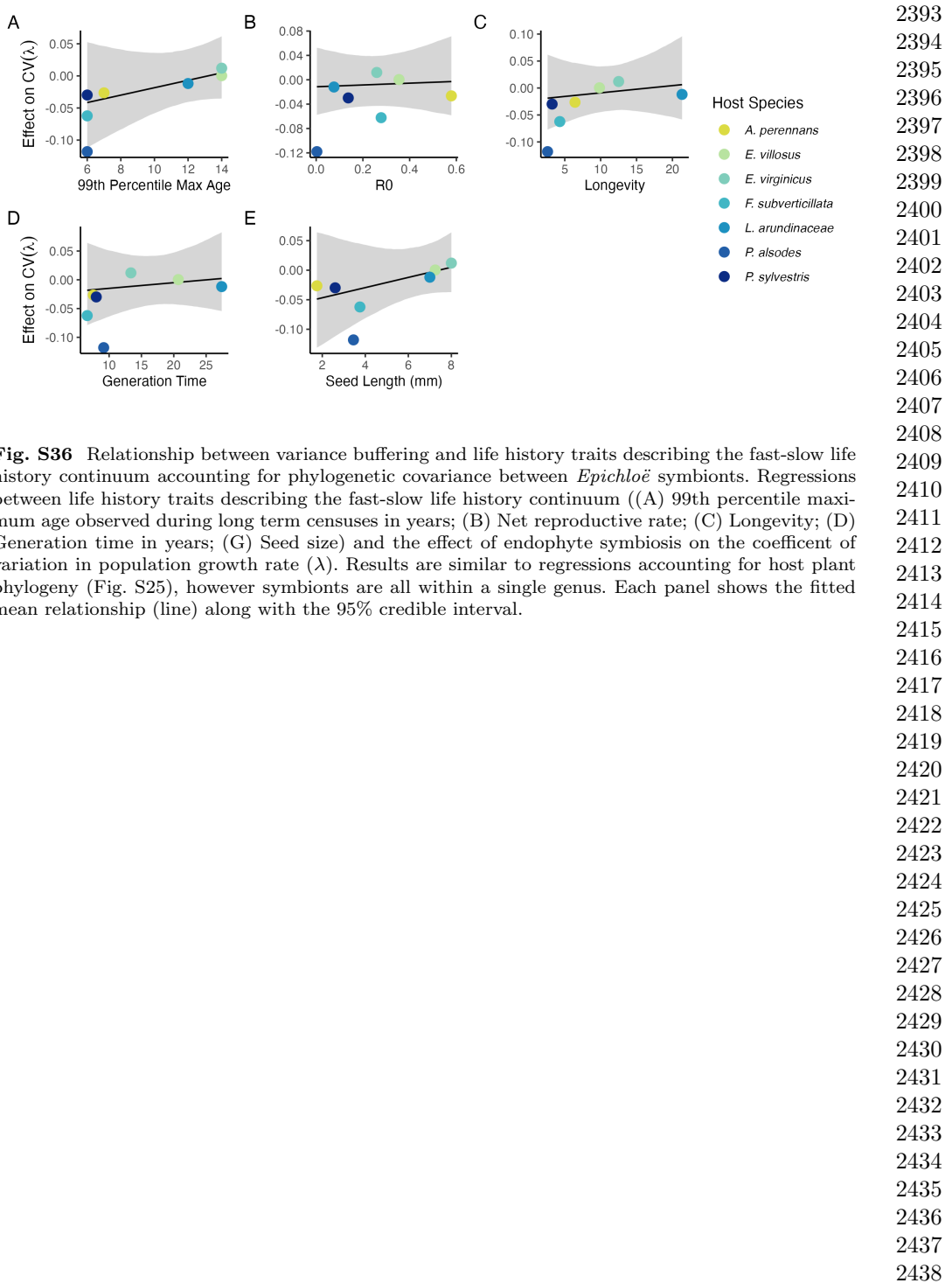


**Fig. S36** Relationship between variance buffering and life history traits describing the fast-slow life history continuum accounting for phylogenetic covariance between *Epichloë* symbionts. Regressions between life history traits describing the fast-slow life history continuum ((A) 99th percentile maximum age observed during long term censuses in years; (B) Net reproductive rate; (C) Longevity; (D) Generation time in years; (E) Seed size) and the effect of endophyte symbiosis on the coefficient of variation in population growth rate ( $\lambda$ ). Results are similar to regressions accounting for host plant phylogeny (Fig. S25), however symbionts are all within a single genus. Each panel shows the fitted mean relationship (line) along with the 95% credible interval.

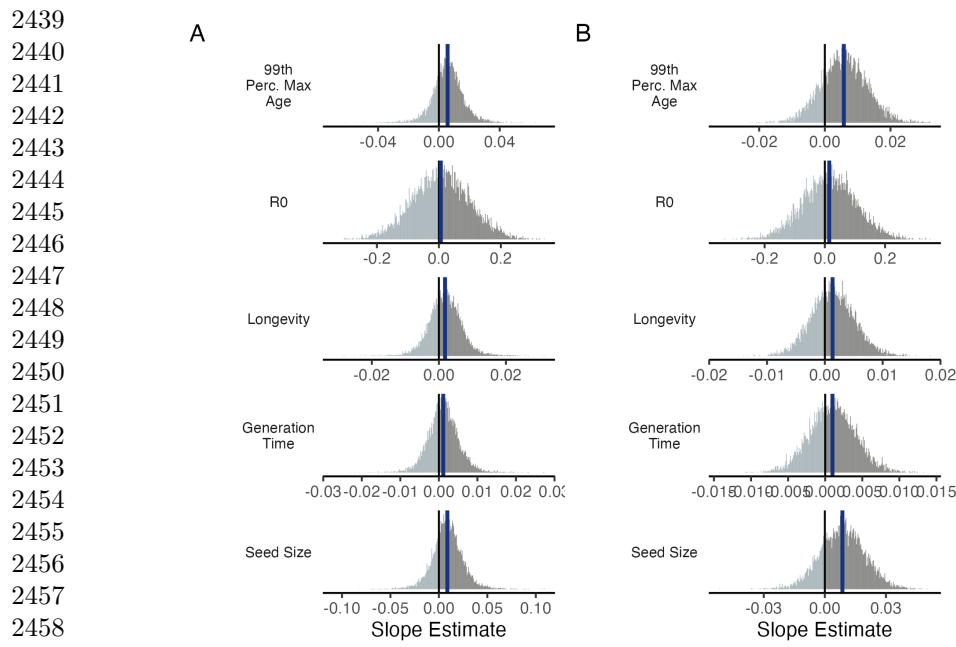


**Fig. S37** Posterior estimates of life history trait effects on variance buffering. Grey histograms show the posterior distribution of the slope parameter from models incorporating (A) host plant phylogenetic covariance and (B) symbiont phylogenetic covariance for each life history trait with blue bars showing the posterior mean.

<b>Supplemental Tables S1-S3</b>	2485
	2486
	2487
	2488
	2489
	2490
	2491
	2492
	2493
	2494
	2495
	2496
	2497
	2498
	2499
	2500
	2501
	2502
	2503
	2504
	2505
	2506
	2507
	2508
	2509
	2510
	2511
	2512
	2513
	2514
	2515
	2516
	2517
	2518
	2519
	2520
	2521
	2522
	2523
	2524
	2525
	2526
	2527
	2528
	2529
	2530

2531  
 2532  
 2533  
 2534  
 2535  
 2536  
 2537  
 2538  
 2539  
 2540  
 2541  
 2542  
 2543  
 2544  
 2545  
 2546  
 2547  
 2548  
 2549  
 2550  
 2551  
 2552  
 2553  
 2554  
 2555  
 2556  
 2557  
 2558  
 2559  
 2560  
 2561  
 2562  
 2563  
 2564  
 2565  
 2566  
 2567  
 2568  
 2569  
 2570  
 2571  
 2572  
 2573  
 2574  
 2575  
 2576

**Table S1** Summary of host-endophyte propagation and transplant methods

Host Species	Symbiont Species	Heat treatment duration (Temp.)	Transplant date
<i>Agrostis perennans</i>	<i>E. amarillans</i>	12 min. hot water bath (60 °C)	April 2008 (10 plots)
<i>Elymus villosus</i>	<i>E. elymi</i>	6 days drying oven (60 °C)	April 2008 (10 plots)
<i>Elymus virginicus</i>	<i>E. elymi</i> or <i>EviTG-1</i>	6 days drying oven (60 °C)	April 2008 (10 plots)
<i>Festuca subverticillata</i>	<i>E. starrii</i>	6 days drying oven (60 °C)	April 2008 (10 plots)
<i>Lolium arundinaceum</i>	<i>E. coenophiala</i>	6 days drying oven (60 °C)	Sept. 2007 (10 plots)
<i>Poa alsodes</i>	<i>E. alsodes</i>	7 days drying oven (60 °C)	Sept. 2007 (8 plots)/April 2008 (10 plots)
<i>Poa sylvestris</i>	<i>E. PsyTG-1</i>	7 days drying oven (60 °C)	Sept. 2007 (8 plots)/April 2008 (10 plots)

**Table S2** Summary of focal life history traits

Host Species	Observed max age (years)	99th percentile max age (years)	Generation time (years)	$R_0$	Longevity (years)	Seed length (mm.)	Imperfect transmission rate (%)	Stromata Observed of indiv. per species)
<i>Agrostis perennans</i>	11	7	7.6	0.58	6.4	1.75	69.8	0.0
<i>Elymus villosus</i>	14	14	20.7	0.35	9.8	7.25	100	4.6
<i>Elymus virginicus</i>	14	14	13.4	0.25	12.5	8	100	0.6
<i>Festuca subverticillata</i>	9	6	6.6	0.28	4.3	3.75	42.7	0.0
<i>Lolium arundinaceum</i>	12*	12*	27.4	0.08	21.3	7	100	0.0
<i>Poa alsodes</i>	8	6	9.2	0.003	2.6	3.45	99.9	0.0
<i>Poa sylvestris</i>	12	6	8.0	0.14	3.2	2.6	16.6	0.1

\*Censuses for *L. arundinaceum* plots stopped after year 12 of the experiment.

2623  
 2624  
 2625  
 2626  
 2627  
 2628  
 2629  
 2630  
 2631  
 2632  
 2633  
 2634  
 2635  
 2636  
 2637  
 2638  
 2639  
 2640  
 2641  
 2642  
 2643  
 2644  
 2645  
 2646  
 2647  
 2648  
 2649  
 2650  
 2651  
 2652  
 2653  
 2654  
 2655  
 2656  
 2657  
 2658  
 2659  
 2660  
 2661  
 2662  
 2663  
 2664  
 2665  
 2666  
 2667  
 2668

**Table S3** Summary of host-endophyte drought sensitivities

Host Species	Effect on CV( $\lambda$ )	Effect on Mean( $\lambda$ )	$\frac{\Delta\lambda^-}{\Delta SPEI_3}$	$\frac{\Delta\lambda^+}{\Delta SPEI_3}$	3 month S- to S+ ratio	$\frac{\Delta\lambda^-}{\Delta SPEI_{12}}$	$\frac{\Delta\lambda^+}{\Delta SPEI_{12}}$	12 month S- to S+ ratio
<i>Agrostis perennans</i>	-0.0264	0.0441	0.03	-0.04	0.85	0.11	-0.06	1.82
<i>Elymus villosus</i>	0.0003	0.0509	-0.03	0.01	1.95	0.03	0.04	0.70
<i>Elymus virginicus</i>	0.0120	0.0578	0.07	0.05	1.50	0.10	0.07	1.42
<i>Festuca subverticillata</i>	-0.0622	0.1639	0.02	0.02	1.01	-0.13	-0.09	1.43
<i>Lolium arundinaceum</i>	-0.0118	0.1022	-0.01	0.01	1.32	0.03	-0.03	1.02
<i>Poa alsodes</i>	-0.1179	0.1282	0.10	0.14	0.71	0.11	0.14	0.73
<i>Poa sylvestris</i>	-0.0298	-0.0085	0.07	0.16	0.44	0.05	0.10	0.55

<b>References</b>	2669
[1] Seneviratne, S. <i>et al.</i> <i>Changes in climate extremes and their impacts on the natural physical environment</i> (Cambridge University Press, 2012).	2670
[2] IPCC. Climate change 2021: The physical science basis (2021). URL <a href="https://www.ipcc.ch/report/ar6/wg1/">https://www.ipcc.ch/report/ar6/wg1/</a> .	2671
[3] Lewontin, R. C. & Cohen, D. On Population Growth in a Randomly Varying Environment. <i>Proceedings of the National Academy of Sciences</i> <b>62</b> , 1056–1060 (1969). URL <a href="https://www.pnas.org/content/62/4/1056">https://www.pnas.org/content/62/4/1056</a> . Publisher: National Academy of Sciences Section: Biological Sciences: Zoology.	2672
[4] Tuljapurkar, S. D. Population dynamics in variable environments. III. Evolutionary dynamics of r-selection. <i>Theoretical Population Biology</i> <b>21</b> , 141–165 (1982). URL <a href="http://www.sciencedirect.com/science/article/pii/0040580982900107">http://www.sciencedirect.com/science/article/pii/0040580982900107</a> .	2673
[5] Cohen, J. E. Comparative statics and stochastic dynamics of age-structured populations. <i>Theoretical population biology</i> <b>16</b> , 159–171 (1979).	2674
[6] Tuljapurkar, S. <i>Population dynamics in variable environments</i> Vol. 85 (Springer Science & Business Media, 2013).	2675
[7] Pfister, C. A. Patterns of variance in stage-structured populations: evolutionary predictions and ecological implications. <i>Proceedings of the National Academy of Sciences</i> <b>95</b> , 213–218 (1998).	2676
[8] Morris, W. F. <i>et al.</i> Longevity can buffer plant and animal populations against changing climatic variability. <i>Ecology</i> <b>89</b> , 19–25 (2008).	2677
[9] Compagnoni, A. <i>et al.</i> The effect of demographic correlations on the stochastic population dynamics of perennial plants. <i>Ecological Monographs</i> <b>86</b> , 480–494 (2016).	2678
[10] Ellis, M. M. & Crone, E. E. The role of transient dynamics in stochastic population growth for nine perennial plants. <i>Ecology</i> <b>94</b> , 1681–1686 (2013).	2679
[11] Rodríguez-Caro, R. C. <i>et al.</i> The limits of demographic buffering in coping with environmental variation. <i>Oikos</i> <b>130</b> , 1346–1358 (2021).	2680
[12] Tuljapurkar, S. & Orzack, S. H. Population dynamics in variable environments i. long-run growth rates and extinction. <i>Theoretical Population Biology</i> <b>18</b> , 314–342 (1980).	2681
[13] Fieberg, J. & Ellner, S. P. Stochastic matrix models for conservation and management: a comparative review of methods. <i>Ecology letters</i> <b>4</b> , 244–266 (2001).	2682
	2683
	2684
	2685
	2686
	2687
	2688
	2689
	2690
	2691
	2692
	2693
	2694
	2695
	2696
	2697
	2698
	2699
	2700
	2701
	2702
	2703
	2704
	2705
	2706
	2707
	2708
	2709
	2710
	2711
	2712
	2713
	2714

- 2715 [14] Menges, E. S. Applications of population viability analyses in plant conservation.  
2716     *Ecological Bulletins* 73–84 (2000).
- 2717  
2718 [15] Kuparinen, A., Boit, A., Valdovinos, F. S., Lassaux, H. & Martinez, N. D.  
2719     Fishing-induced life-history changes degrade and destabilize harvested ecosystems.  
2720     *Scientific reports* **6**, 22245 (2016).
- 2721  
2722 [16] Hilde, C. H. *et al.* The Demographic Buffering Hypothesis: Evidence and Chal-  
2723     lenges. *Trends in Ecology & Evolution* **0** (2020). URL [https://www.cell.com/trends/ecology-evolution/abstract/S0169-5347\(20\)30050-1](https://www.cell.com/trends/ecology-evolution/abstract/S0169-5347(20)30050-1). Publisher: Elsevier.
- 2724  
2725 [17] Rodriguez, R., White Jr, J., Arnold, A. E. & Redman, a. R. a. Fungal endophytes:  
2726     diversity and functional roles. *New phytologist* **182**, 314–330 (2009).
- 2727  
2728 [18] McFall-Ngai, M. *et al.* Animals in a bacterial world, a new imperative for the  
2729     life sciences. *Proceedings of the National Academy of Sciences* **110**, 3229–3236  
2730     (2013).
- 2731  
2732 [19] Funkhouser, L. J. & Bordenstein, S. R. Mom knows best: the universality of  
2733     maternal microbial transmission. *PLoS biology* **11**, e1001631 (2013).
- 2734  
2735 [20] Fine, P. E. Vectors and vertical transmission: an epidemiologic perspective.  
2736     *Annals of the New York Academy of Sciences* **266**, 173–194 (1975).
- 2737  
2738 [21] Russell, J. A. & Moran, N. A. Costs and benefits of symbiont infection in aphids:  
2739     variation among symbionts and across temperatures. *Proceedings of the Royal  
2740     Society B: Biological Sciences* **273**, 603–610 (2006).
- 2741  
2742 [22] Kivlin, S. N., Emery, S. M. & Rudgers, J. A. Fungal symbionts alter plant  
2743     responses to global change. *American Journal of Botany* **100**, 1445–1457 (2013).
- 2744  
2745 [23] Dunbar, H. E., Wilson, A. C. C., Ferguson, N. R. & Moran, N. A. Aphid thermal  
2746     tolerance is governed by a point mutation in bacterial symbionts. *PLoS biology*  
2747     **5**, e96 (2007).
- 2748  
2749 [24] Reyna, R., Cooke, P., Grum, D., Cook, D. & Creamer, R. Detection and local-  
2750     ization of the endophyte *undifilum oxytropis* in locoweed tissues. *Botany* **90**,  
2751     1229–1236 (2012).
- 2752  
2753 [25] Saikkonen, K., Gundel, P. E. & Helander, M. Chemical ecology mediated by  
2754     fungal endophytes in grasses. *Journal of chemical ecology* **39**, 962–968 (2013).
- 2755  
2756 [26] Neyaz, M., Gardner, D. R., Creamer, R. & Cook, D. Localization of the  
2757     swainsonine-producing chaetothyriales symbiont in the seed and shoot apical  
2758     meristem in its host *ipomoea carnea*. *Microorganisms* **10**, 545 (2022).
- 2759  
2760 [27] Chamberlain, S. A., Bronstein, J. L. & Rudgers, J. A. How context dependent  
2761     are species interactions? *Ecology letters* **17**, 881–890 (2014).

- [28] Jordano, P. Spatial and temporal variation in the avian-frugivore assemblage of prunus mahaleb: patterns and consequences. *Oikos* **479–491** (1994). 2761  
2762  
2763
- [29] Leuchtmann, A. Systematics, distribution, and host specificity of grass endophytes. *Natural toxins* **1**, 150–162 (1992). 2764  
2765  
2766
- [30] Cheplick, G. P., Faeth, S. & Faeth, S. H. *Ecology and evolution of the grass-endophyte symbiosis* (OUP USA, 2009). 2767  
2768  
2769
- [31] Brem, D. & Leuchtmann, A. Epichloë grass endophytes increase herbivore resistance in the woodland grass brachypodium sylvaticum. *Oecologia* **126**, 522–530 (2001). 2770  
2771  
2772  
2773
- [32] Decunta, F. A., Pérez, L. I., Malinowski, D. P., Molina-Montenegro, M. A. & Gundel, P. E. A systematic review on the effects of epichloë fungal endophytes on drought tolerance in cool-season grasses. *Frontiers in plant science* **12**, 644731 (2021). 2774  
2775  
2776  
2777
- [33] Bacon, C. W. & White, J. F. in *Stains, media, and procedures for analyzing endophytes* 47–56 (CRC Press, 2018). 2778  
2779  
2780
- [34] Rudgers, J. A. & Swafford, A. L. Benefits of a fungal endophyte in elymus virginicus decline under drought stress. *Basic and Applied Ecology* **10**, 43–51 (2009). 2781  
2782  
2783  
2784
- [35] Bultman, T. L., White Jr, J. F., Bowdish, T. I., Welch, A. M. & Johnston, J. Mutualistic transfer of epichloë spermatia by phorbis flies. *Mycologia* **87**, 182–189 (1995). 2785  
2786  
2787  
2788
- [36] Stan Development Team. RStan: the R interface to Stan (2022). URL <https://mc-stan.org/>. R package version 2.21.7. 2789  
2790  
2791
- [37] Elderd, B. D. & Miller, T. E. Quantifying demographic uncertainty: Bayesian methods for integral projection models. *Ecological Monographs* **86**, 125–144 (2016). 2792  
2793  
2794
- [38] Gabry, J., Simpson, D., Vehtari, A., Betancourt, M. & Gelman, A. Visualization in bayesian workflow. *Journal of the Royal Statistical Society Series A: Statistics in Society* **182**, 389–402 (2019). 2795  
2796  
2797  
2798
- [39] Brooks, S. P. & Gelman, A. General methods for monitoring convergence of iterative simulations. *Journal of computational and graphical statistics* **7**, 434–455 (1998). 2799  
2800  
2801  
2802
- [40] Gelman, A. & Hill, J. *Data analysis using regression and multilevel/hierarchical models* (Cambridge university press, 2006). 2803  
2804  
2805  
2806

- 2807 [41] Williams, J. L., Miller, T. E. & Ellner, S. P. Avoiding unintentional eviction from  
2808 integral projection models. *Ecology* **93**, 2008–2014 (2012).
- 2809
- 2810 [42] Jones, O. R. *et al.* Rcompadre and rage—two r packages to facilitate the use of  
2811 the compadre and comadre databases and calculation of life-history traits from  
2812 matrix population models. *Methods in Ecology and Evolution* **13**, 770–781 (2022).
- 2813
- 2814 [43] .
- 2815 [44] Bürkner, P.-C. brms: An R package for Bayesian multilevel models using Stan.  
2816 *Journal of Statistical Software* **80**, 1–28 (2017).
- 2817
- 2818 [45] Zanne, A. E. *et al.* Three keys to the radiation of angiosperms into freezing  
2819 environments. *Nature* **506**, 89–92 (2014).
- 2820
- 2821 [46] Leuchtmann, A., Bacon, C. W., Schardl, C. L., White Jr, J. F. & Tadych,  
2822 M. Nomenclatural realignment of neotyphodium species with genus epichloë.  
2823 *Mycologia* **106**, 202–215 (2014).
- 2824
- 2825 [47] Metcalf, C. J. E. *et al.* Statistical modelling of annual variation for inference  
2826 on stochastic population dynamics using integral projection models. *Methods in  
2827 Ecology and Evolution* **6**, 1007–1017 (2015).
- 2828
- 2829 [48] Caswell, H. Matrix population models: Construction, analysis, and interpretation.  
2830 2nd edn sinauer associates. Inc., Sunderland, MA (2001).
- 2831
- 2832 [49] Rees, M. & Ellner, S. P. Integral projection models for populations in temporally  
2833 varying environments. *Ecological Monographs* **79**, 575–594 (2009).
- 2834
- 2835 [50] Vicente-Serrano, S. M., Beguería, S. & López-Moreno, J. I. A multiscalar drought  
2836 index sensitive to global warming: the standardized precipitation evapotranspi-  
2837 ration index. *Journal of climate* **23**, 1696–1718 (2010).
- 2838
- 2839 [51] Rudgers, J. A. & Clay, K. An invasive plant–fungal mutualism reduces arthropod  
2840 diversity. *Ecology Letters* **11**, 831–840 (2008).
- 2841
- 2842 [52] Crawford, K. M., Land, J. M. & Rudgers, J. A. Fungal endophytes of native  
2843 grasses decrease insect herbivore preference and performance. *Oecologia* **164**,  
2844 431–444 (2010).
- 2845
- 2846 [53] Murphy, G. I. Pattern in life history and the environment. *The American  
2847 Naturalist* **102**, 391–403 (1968).
- 2848
- 2849 [54] Compagnoni, A. *et al.* Herbaceous perennial plants with short generation time  
2850 have stronger responses to climate anomalies than those with longer generation  
time. *Nature communications* **12**, 1–8 (2021).
- 2851
- 2852

- [55] Le Coeur, C., Yoccoz, N. G., Salguero-Gómez, R. & Vindenes, Y. Life history adaptations to fluctuating environments: Combined effects of demographic buffering and lability. *Ecology Letters* **25**, 2107–2119 (2022). 2853  
2854  
2855  
2856  
2857  
2858  
2859  
2860  
2861  
2862  
2863  
2864  
2865  
2866  
2867  
2868  
2869  
2870  
2871  
2872  
2873  
2874  
2875  
2876  
2877  
2878  
2879  
2880  
2881  
2882  
2883  
2884  
2885  
2886  
2887  
2888  
2889  
2890  
2891  
2892  
2893  
2894  
2895  
2896  
2897  
2898
- [56] Rees, M. Evolutionary ecology of seed dormancy and seed size. *Philosophical Transactions of the Royal Society of London. Series B: Biological Sciences* **351**, 1299–1308 (1996). 2853  
2854  
2855  
2856  
2857  
2858  
2859  
2860  
2861  
2862  
2863  
2864  
2865  
2866  
2867  
2868  
2869  
2870  
2871  
2872  
2873  
2874  
2875  
2876  
2877  
2878  
2879  
2880  
2881  
2882  
2883  
2884  
2885  
2886  
2887  
2888  
2889  
2890  
2891  
2892  
2893  
2894  
2895  
2896  
2897  
2898
- [57] Moles, A. T. & Westoby, M. Seedling survival and seed size: a synthesis of the literature. *Journal of Ecology* **92**, 372–383 (2004). 2860  
2861  
2862  
2863  
2864  
2865  
2866  
2867  
2868  
2869  
2870  
2871  
2872  
2873  
2874  
2875  
2876  
2877  
2878  
2879  
2880  
2881  
2882  
2883  
2884  
2885  
2886  
2887  
2888  
2889  
2890  
2891  
2892  
2893  
2894  
2895  
2896  
2897  
2898
- [58] Afkhami, M. E. & Rudgers, J. A. Symbiosis lost: imperfect vertical transmission of fungal endophytes in grasses. *The American Naturalist* **172**, 405–416 (2008). 2860  
2861  
2862  
2863  
2864  
2865  
2866  
2867  
2868  
2869  
2870  
2871  
2872  
2873  
2874  
2875  
2876  
2877  
2878  
2879  
2880  
2881  
2882  
2883  
2884  
2885  
2886  
2887  
2888  
2889  
2890  
2891  
2892  
2893  
2894  
2895  
2896  
2897  
2898
- [59] Jeschke, J. M. & Kokko, H. The roles of body size and phylogeny in fast and slow life histories. *Evolutionary Ecology* **23**, 867–878 (2009). 2860  
2861  
2862  
2863  
2864  
2865  
2866  
2867  
2868  
2869  
2870  
2871  
2872  
2873  
2874  
2875  
2876  
2877  
2878  
2879  
2880  
2881  
2882  
2883  
2884  
2885  
2886  
2887  
2888  
2889  
2890  
2891  
2892  
2893  
2894  
2895  
2896  
2897  
2898
- [60] Afkhami, M. E. & Strauss, S. Y. Native fungal endophytes suppress an exotic dominant and increase plant diversity over small and large spatial scales. *Ecology* **97**, 1159–1169 (2016). 2860  
2861  
2862  
2863  
2864  
2865  
2866  
2867  
2868  
2869  
2870  
2871  
2872  
2873  
2874  
2875  
2876  
2877  
2878  
2879  
2880  
2881  
2882  
2883  
2884  
2885  
2886  
2887  
2888  
2889  
2890  
2891  
2892  
2893  
2894  
2895  
2896  
2897  
2898
- [61] Smith, E., Vaughan, G., Ketchum, R., McParland, D. & Burt, J. Symbiont community stability through severe coral bleaching in a thermally extreme lagoon. *Scientific Reports* **7**, 2428 (2017). 2860  
2861  
2862  
2863  
2864  
2865  
2866  
2867  
2868  
2869  
2870  
2871  
2872  
2873  
2874  
2875  
2876  
2877  
2878  
2879  
2880  
2881  
2882  
2883  
2884  
2885  
2886  
2887  
2888  
2889  
2890  
2891  
2892  
2893  
2894  
2895  
2896  
2897  
2898
- [62] Dallas, J. W. & Warne, R. W. Captivity and animal microbiomes: potential roles of microbiota for influencing animal conservation. *Microbial Ecology* 1–19 (2022). 2860  
2861  
2862  
2863  
2864  
2865  
2866  
2867  
2868  
2869  
2870  
2871  
2872  
2873  
2874  
2875  
2876  
2877  
2878  
2879  
2880  
2881  
2882  
2883  
2884  
2885  
2886  
2887  
2888  
2889  
2890  
2891  
2892  
2893  
2894  
2895  
2896  
2897  
2898
- [63] Wu, L. *et al.* Reduction of microbial diversity in grassland soil is driven by long-term climate warming. *Nature Microbiology* **7**, 1054–1062 (2022). 2860  
2861  
2862  
2863  
2864  
2865  
2866  
2867  
2868  
2869  
2870  
2871  
2872  
2873  
2874  
2875  
2876  
2877  
2878  
2879  
2880  
2881  
2882  
2883  
2884  
2885  
2886  
2887  
2888  
2889  
2890  
2891  
2892  
2893  
2894  
2895  
2896  
2897  
2898
- [64] Ehrlén, J. & Morris, W. F. Predicting changes in the distribution and abundance of species under environmental change. *Ecology letters* **18**, 303–314 (2015). 2860  
2861  
2862  
2863  
2864  
2865  
2866  
2867  
2868  
2869  
2870  
2871  
2872  
2873  
2874  
2875  
2876  
2877  
2878  
2879  
2880  
2881  
2882  
2883  
2884  
2885  
2886  
2887  
2888  
2889  
2890  
2891  
2892  
2893  
2894  
2895  
2896  
2897  
2898
- [65] Chamberlain, S., Hocking, D. & Anderson, B. Package ‘rnoaa’ (2022). 2860  
2861  
2862  
2863  
2864  
2865  
2866  
2867  
2868  
2869  
2870  
2871  
2872  
2873  
2874  
2875  
2876  
2877  
2878  
2879  
2880  
2881  
2882  
2883  
2884  
2885  
2886  
2887  
2888  
2889  
2890  
2891  
2892  
2893  
2894  
2895  
2896  
2897  
2898
- [66] Beguería, S. & Vicente-Serrano, S. M. Spei: calculation of the standardised precipitation-evapotranspiration index. *R package version* **1** (2013). 2860  
2861  
2862  
2863  
2864  
2865  
2866  
2867  
2868  
2869  
2870  
2871  
2872  
2873  
2874  
2875  
2876  
2877  
2878  
2879  
2880  
2881  
2882  
2883  
2884  
2885  
2886  
2887  
2888  
2889  
2890  
2891  
2892  
2893  
2894  
2895  
2896  
2897  
2898